4-2016

The Decomposition of Hydroxylammonium Nitrate under Vacuum Conditions

Gregory A. Neff
Western Michigan University

THE DECOMPOSITION OF HYDROXYLAMMONIUM NITRATE UNDER VACUUM CONDITIONS

by

Gregory A. Neff

A thesis submitted to the Graduate College
in partial fulfillment of the requirements
for the degree of Master of Science in Engineering (Mechanical)
Mechanical and Aerospace Engineering
Western Michigan University
April 2016

Thesis Committee:

Kristina M. Lemmer, Ph.D., Chair
Bade Shrestha, Ph.D.
Ramakrishna Guda, Ph.D.

THE DECOMPOSITION OF HYDROXYLAMMONIUM NITRATE UNDER VACUUM CONDITIONS

Gregory A. Neff, M.S.E.

Western Michigan University, 2016

This research investigates the decomposition of the ionic liquid: hydroxylammonium nitrate (HAN), under vacuum conditions. All research was conducted at the Aerospace Laboratory for Plasma Experiments (ALPE) at Western Michigan University. Hydroxylammonium nitrate solution 24% wt. in H_2O was used consistently throughout this research. A variety of temperatures and pressures ranging from 23°C to 645°C and 6E-3 Torr to 4 Torr, respectively, were used to decompose HAN. The primary gaseous species resulting from these decomposition conditions are N_2O, NO, and trace amounts of NO_2. The formation of H_2O, and N_2 is conditional on the experimental conditions, and the formation of HNO_3 was also observed. A Residual Gas Analyzer with a range of 300 atomic mass units was used as the primary diagnostic for this research.

ACKNOWLEDGEMENTS

None of this would have been possible without the continuing support of my family, friends and colleagues. I moved out to Kalamazoo, certainly for the engineering department at WMU, but also to be with my grandparents, Rose-Marie and F. Claus Globig, who have always been a big part of my life.

I am grateful for the valuable time I was able to spend with my grandmother before she passed in 2014. Having her love and support right around the corner made my decision to study at Western one of the best decisions of my life. My grandfather, Dr. F. Claus Globig, also an engineer, inspired me from an early age to be a thinker and man of science. He taught me the importance of having a solid understanding of how things work in the world. To this day, he, along with the memory of my grandmother, continue to motivate my higher educational goals and without them, I would not be here today.

My parents, Isabel and Frederick Neff, are doctors of psychology. Their love and guidance in all areas of my life has been unconditional. I thank them for being the best parents as well as for helping me financially so that I could stay focused on my studies. My older sister, Nicole, is a motivation by showing me how important it is to follow your dreams and do what makes you happy. She has always given me validation and encouragement, which has helped me stay the course and go further in my education. Thank you! I also wish to thank my aunts and uncle for being there for me in so many ways.

Furthermore, none of this would have been possible without the support and mentorship that Dr. Kristina Lemmer has provided over the years. I first started working for Dr. Lemmer by sorting out her tools and equipment before she had a lab to put them in. She has since helped me attain two amazing internships at NASA and the Air Force Research Laboratory, as well as procured the funding for this research. I am proud to have helped create the Aerospace Laboratory for Plasma Experiments (I think we picked a good name) and I look forward to seeing what it accomplishes down the road. Thank you, Dr. Lemmer for believing in me and my abilities. It has been fun and a pleasure!

Lastly, of course, I wish to thank my friends and lab mates, who, over the years have been there for me in countless ways. I appreciate your help by being there when I needed to talk through my research thoughts and to listen to my complaints when things did not work out as planned. Also, thank you to everyone I have met in the aerospace and electric propulsion field who kept me inspired.

Gregory A. Neff

TABLE OF CONTENTS

Table of Contents – Continued

CHAPTER

LIST OF TABLES

LIST OF FIGURES

List of Figures – Continued

NOMENCLATURE

Symbol	Description
A	Absorbance
A_e	Exit area of nozzle
c	Concentration of sample
CO	Carbon dioxide
$\varepsilon(\tilde{\nu})$	Molar absorbance coefficient
F	Force
H_2	Hydrogen
HNO	Nitroxyl
HNO_2	Nitrous acid
HNO_3	Nitric acid
H_2O	Water
H_3NO_2	Intermediate dihydroxyamine
I	Irradiated intensity
I_o	Incident intensity
I_{sp}	Specific impulse
l	Length
$\dot{m}$	Mass flow rate
N_2H_2	Hydrazine
NH_2OH	Hydroxylamine

Nomenclature – Continued

Symbol	Description
N_2	Nitrogen
N_2O	Nitrous oxide
NO	Nitric oxide
NO_2	Nitrogen dioxide
O	Molecular oxygen
O_2	Oxygen
OH	Hydroxide
p_e	Pressure at nozzle exit
p_o	Pressure of atmosphere
u_e	Exit velocity

CHAPTER I

INTRODUCTION

Research Motivation

There is a growing interest in developing a spacecraft propulsion system that increases mission capability and versatility. A dual-mode propulsion system would utilize one propellant storage tank and management system that would feed separate thrusters depending on the type of maneuver required. This propulsion system would incorporate both high thrust, low efficiency chemical propulsion as well as high efficiency, low thrust electric propulsion. With the cost of missions continually increasing, mission capability would increase without the added cost of dual storage tanks and propellant management systems that would otherwise be required for a dual-mode propulsion system with current technology. The development of a cost-effective dual-mode propulsion system requires a propellant that can be used as both a monopropellant, as well as the propellant for an electric propulsion device.

Currently, there are two types of commonly used space propulsion, chemical propulsion and electric propulsion, and they use very different types of propellant. Chemical propulsion is commonly in the form of hydrogen-liquid oxygen engines, solid rocket boosters, and hydrazine (N_2H_4) monopropellant thrusters. Monopropellant thrusters, see Figure 1, are high thrust chemical engines that do not require a secondary liquid such as an oxidizer to complete the chemical reaction and are therefore the preferred means of chemical propulsion used for attitude control, orbit transfers, and orbital inclination changes once in space [1].

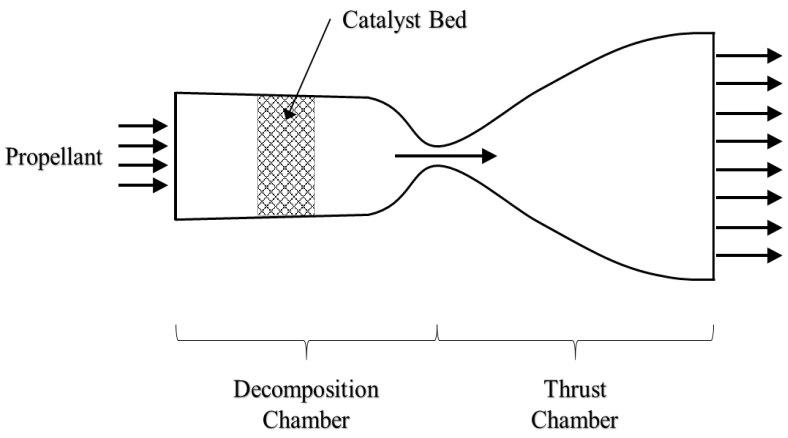

Figure 1: Monopropellant thruster diagram

Monopropellants are passed over a catalyst bed, and the resulting exothermic reaction is expanded through a traditional converging diverging nozzle to generate maximum thrust.

Electric propulsion, also known as 'EP', is used for orbital maneuvers, but with much greater efficiency, unlike conventional chemical propulsion. Efficiency of space propulsion is generally described in terms of I_{sp}, or specific impulse. Chemical propulsion using a liquid bipropellant generally has an I_{sp} of 290-460 s with relatively high thrust, and chemical propulsion that uses a liquid monopropellant has an I_{sp} of 150-290 s [2]. Electric Propulsion can have an I_{sp} upwards of 3000 s, but with thrust at the millinewton level [2]. Both chemical and electric propulsion follow the thrust equation as seen in Equation 1,

$$F = \dot{m}u_e + A_e(p_e - p_o) \tag{1}$$

Where F is the thrust, $\dot{m}$ is the mass flow rate of propellant leaving the propulsion device, u_e is the exit velocity, A_e is the exit area of the nozzle, and $p_e - p_o$ is the pressure difference between the exit of the nozzle and atmosphere. For chemical propulsion, high thrust is generated by moving a large mass at somewhat high velocities, coupled with the pressure difference. In contrast, electric

propulsion generates its thrust from accelerating ionized gas (usually a Nobel gas such as xenon), called plasma, to speeds upwards of 30 km/s. The low mass, high velocity plasma generates small amounts of thrust, and the difference in pressure is negated due to the insignificant pressure difference between the thruster exit plane and the vacuum of space. There are a variety of electric propulsion devices with the best known being Hall thrusters and ion thrusters. The type of EP systems that would most likely be used for a dual-mode propulsion device is a Field Reversed Configuration (FRC) thruster. This is because there is minimal interaction with the propellant and thruster surfaces.

Current monopropellant thrusters use a propellant called hydrazine (N_2H_4). This particular propellant has had great success in the past. However, hydrazine is very toxic. The combination of toxicity and high vapor pressure leads to expensive storage and handling costs [3], [4]. Current research is being focused on ionic liquids as the best alternative for hydrazine [5]. Hydroxylammonium nitrate (HAN) is an ionic liquid that is highly sought after, due to its low freezing point, high density, low environmental impact, and absence of noticeable vapor pressure below 65°C [6]–[8]. HAN-based ionic liquids are known as 'green monopropellants' for the aforementioned reasons. Ionic liquids have improved properties over hydrazine for space environments, and they are easier to work with because they are more stable and less toxic [9]. Additionally, HAN's higher density allows for a smaller storage tank onboard a spacecraft, thus reducing weight and cost [4], [10]. Hydrazine and HAN-based monopropellants have comparable I_{sp} around 220 and 270 s respectively, with HAN tending to be slightly higher depending on the other components that make up the monopropellant mixture [11], [12]. Therefore, HAN-based propellants are being heavily investigated as a hydrazine alternative [10].

In addition to using HAN-based propellants in monopropellant thrusters, there is also interest in using them as the propellant for EP devices. Therefore, a dual-use monopropellant can be both burned inside a catalyst chamber for high thrust and low I_{sp}, as well as decomposed into gaseous components and ionized using electric propulsion techniques for low thrust and high I_{sp}.

The decomposition of HAN under vacuum conditions has not specifically been studied. The understanding of resultant gasses produced from decomposition is vital for the development of a gas-phase EP device. Furthermore, understanding the ionized decomposition gases is important for the development of a gas-phase EP device. The decomposition products of HAN are the gases that make up the gas-phase EP thruster's propellant. The type of propellant used determines power requirements, size, materials used, and possible mission capabilities of the EP device. Therefore, the decomposition products of HAN under vacuum conditions must be studied.

Research Significance

Although the decomposition of HAN has been studied for many years, previous research has not focused on using ionic liquids as a propellant in gas-phase EP devices. This research differs significantly, as it focuses on the decomposition of HAN under vacuum conditions that are similar to conditions in which an EP device must operate. This thesis, therefore, contributes to the development of a gas-phase ionic liquid electric thruster in the following manner:

1. Decomposition Chamber: A method and experimental setup was designed and employed in which various liquids, including ionic liquids, can be introduced into varying levels of vacuum. The setup is capable of decomposing liquids under select levels of heat addition and in the presence of inert gases if desired.

2. HAN Phase Changes: HAN, like any liquid, has specific behaviors when exposed to vacuum, heat, or the combination of both. The states of HAN as exposed to these conditions are reported and discussed.
3. Results: The results of this research will yield insight into the development of a dual-mode propulsion system by providing decomposition results from a variety of conditions.

Organization

This thesis is organized as follows: The first section introduces the research topic and explains why such research is needed. The introduction is followed by the literature review, which relates to the research presented in this paper to previous research and explains how this research differs from previous work. Then, the thesis advances to an explanation of the diagnostic tools employed and the experimental setup is explained. Finally, the experimental results are presented and discussed, along with future work and recommendations.

1. Introduction: The introduction describes the motivation behind the research, as well as the deliverables and contributions.
2. Literature Review: This section explains the background on HAN. This review describes the previous uses of HAN, how this HAN is understood to decompose initially, and some of the proposed global reactions that take place. Lastly, the decomposition products from past experiments are presented.
3. Diagnostics: This section explains what diagnostic tools were used for this research, how they work, and what considerations must be used when analyzing the results of the data.
4. Experimental Setup: The experimental setup is explained in this chapter. First, the vacuum chamber and associated equipment are described. Next, the specialized decomposition

chamber is discussed as experimental setup 1 and 1B, and the vacuum chamber decomposition as experimental setup 2.

5. Experimental Results: In this section, all experimental results are shown. A brief explanation is also provided alongside the conditions in which the decomposition occurred.
6. Conclusion: The experimental results are discussed and compared. Further extrapolation of the data is also used to create an overall model of HAN's behavior under varying environments. Future work and recommendations are also discussed.

CHAPTER II

LITERATURE REVIEW

HAN Properties

HAN is a salt containing a single cation and anion as seen below in Figure 2 [13]. HAN is classified as an oxidizer with an oxygen balance of 33.33% and it is most commonly used as the oxidizer component in propellants; however, it can be a monopropellant by itself [1], [2], [12], [14]. Under standard temperature and pressure, this salt can be dissolved up to 95% by weight in water [2], [14]. Pure HAN has a density of approximately 1.83 g/cm^3, whereas hydrazine is about 1.01 g/cm^3. The melting point of HAN is around 43˚C [1], [15]. A HAN-water mixture is a clear liquid with no noticeable vapor pressure at standard temperature and pressure [6], [8]. Most HAN-based monopropellants are mixtures of HAN, water, and a fuel; therefore, the density is slightly lower than its pure form. Regardless, the density of the mixture remains higher than hydrazine [11].

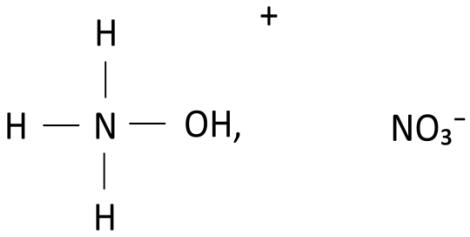

Figure 2: Chemical structure of HAN

HAN Background

HAN has been studied for over 30 years for its potential use as a Liquid Gun Propellant (LGP) [1]. The Army developed LP1846 and LP1845, which are homogenous mixtures of HAN, triethanolammonium nitrate (TEAN), and water, as well as LP1898 which is a mixture of HAN,

diethylhydroxylammonium nitrate (DEHAN), and water [11]. The successful implementation of these propellants would have resulted in caseless ammunition and an increase in muzzle velocity [16]. However, a report on liquid guns concluded that HAN-based LGPs presented a number of problems [16]. To name a few, it was concluded that the act of pumping the LGP would increase the possibility of propellant contamination. And varying temperature conditions would result in a change in viscosity that would vary the performance of the gun [16]. Interestingly, HAN-based propellants presented other qualities which were attractive for their application to space propulsion [11], [16]. Even though these HAN-based propellants were no longer considered as LGPs, HAN became a possible replacement option to state-of-the-art hydrazine [1], [11].

HAN has also been studied as a reducing agent for plutonium and for decontamination in the nuclear industry [17]–[19]. The use of HAN in this application is believed to have caused vessel ruptures and several explosions due to the unstable nature and auto-catalytic affects that are inherent with HAN [20], [21]. Due to HAN's prominence in the nuclear industry, as well as various incidents, the decomposition pathway and thermal stability [17], [19], [22], [23] as well as the metal ion catalytic effects [18] have been investigated significantly. These previous studies have reported on global decomposition reactions as well as the storage and stability of HAN [17].

More recently, studies have been done on the decomposition and storability of HAN-based monopropellants for their application in chemical propulsion [4], [6], [7], [12], [24], [25]. These papers report on the catalytic decomposition, as well as the thermal decomposition.

HAN Decomposition

It has been observed, and generally agreed upon, that the decomposition of HAN begins as shown in Reaction 1 [13], [19], [26], [27].

$$NH_3OH^+ NO_3^- \leftrightarrow NH_2OH + HNO_3 \quad \text{(R1)}$$

The proton transfer results in an aqueous solution of HAN in equilibrium with hydroxylamine (NH_2OH) and nitric acid (HNO_3). The specific combination of temperature and HAN concentration in which this process begins is unclear. However, water is noted to be a stabilizing agent for HAN in solution [4]. Therefore, as water is removed (i.e. through an increase in temperature or reduction in pressure) and the concentration of HAN increases, the activation energy needed for decomposition decreases [16], [18]. Furthermore, as water is removed, the concentration of hydroxylamine and nitric acid increases, resulting in a less stable solution. Despite the solution becoming more acidic, hydroxylamine is a stronger base than water, and will therefore associate with the protons released from the nitric acid and keep the solution from its self-catalytic phase. A further increase in temperature and concentration will result in Reaction 2 [26].

$$NH_2OH + HNO_3 \leftrightarrow HNO_2 + HNO + H_2O \quad \text{(R2)}$$

Reaction 2 itself is not auto-catalytic. However, the reaction produces HNO_2 which is identified as the intermediate that leads to auto-catalytic behavior [23]. As HNO_2 is formed, the decomposition of HAN becomes accelerated [27]. Below in Reaction 3, the overall auto-catalytic reaction is shown by the production of HNO_2 from a reaction involving HNO_2 [22].

$$2HNO_2 + NH_2OH \rightarrow 3HNO_2 + H_2O \quad \text{(R3)}$$

This auto-catalytic behavior results in a highly exothermic reaction, which begins only when the majority of water has been removed, resulting in pure liquid HAN (at 48°C) [4], [7], [17], [27]. A diagram representing a decomposition mechanism of HAN adopted from Wei's doctoral dissertation can be seen below in Figure [23]. The underlined species in the figure are final

products; the species in red is auto-catalytic; NH_2OH is hydroxylamine; solid lines represent dominant steps; and dashed lines represent less dominant steps [23].

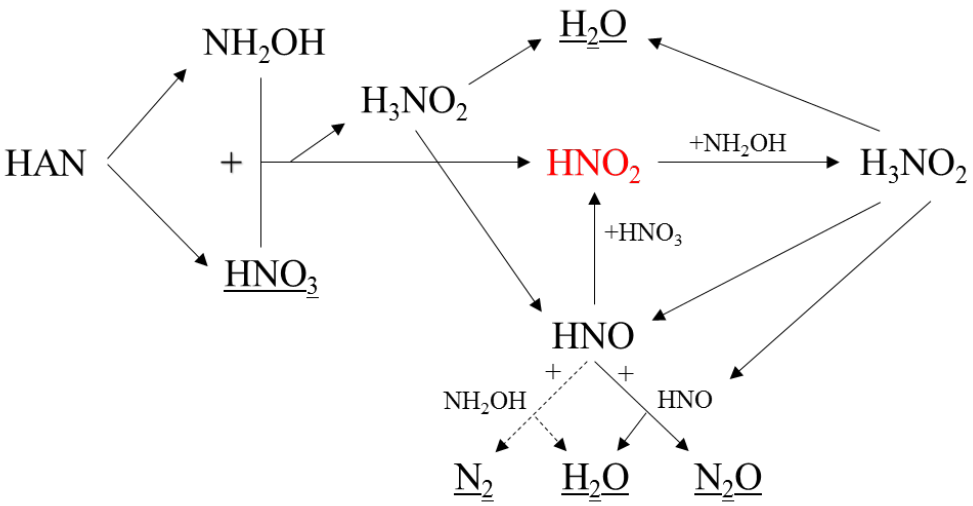

Figure 3: Detailed mechanism of HAN decomposition

Similarly, Oxley and Brower proposed two equations, Reaction 4 and Reaction 5, of equal importance to account for observed quantities from the decomposition of HAN [19].

$$3\,NH_3OH^+\,NO_3^- \rightarrow\ N_2O + N_2 + 2\,HNO_3 + 5\,H_2O \qquad \text{(R4)}$$

$$4\,NH_3OH^+\,NO_3^- \rightarrow\ 3\,N_2O + 2\,HNO_3 + 7\,H_2O \qquad \text{(R5)}$$

Oxley and Brower also determined that a sudden appearance of NO_2 and a darkening of the HAN sample signaled the completion of the reaction. They concluded that the formation of NO_2 and NO were formed from the decomposition of HNO_3 or HNO_2, and therefore not considered in the overall reactions R4 and R5 [19].

Experiments were also conducted in which hydroxylamine was decomposed in nitric acid, HNO_3, where nitric acid was in excess. It was demonstrated that a greater presence of nitric acid increases the rate of HAN decomposition [13]. It is also worth noting that the presence of iron

ions in a HAN solution can have an adverse effect on the stability of HAN by lowering the temperature needed for decomposition [4].

Decomposition Results

The temperature at which thermal decomposition of HAN occurs is a function of HAN concentration and can therefore vary greatly between experiments. However, the experiments result in similar gaseous species. Thermal decomposition of HAN conducted at atmospheric pressure, by Lee and Litzinger, in a nitrogen environment and temperatures around 200°C, resulted in the gaseous species HNO_3, N_2O, NO, and NO_2 [8], [26]. They used Fourier Transform Infrared Spectroscopy (FT-IR) to investigate the decomposition of aqueous HAN. Dijk and Priest observed NO, N_2O, and NO_2 using Raman spectroscopy when decomposing HAN thermally at 180°C and pressures in the range of 100s of kPa [14]. L. Courthéoux et al., using a mass spectrometer, demonstrated that NO_2, N_2O, and NO were produced from thermal decomposition at 174°C and 1 bar of Argon [4]. Oxley and Brower reported that HAN thermally decomposed in initially evacuated glass capillaries at 129°C-139°C into predominantly N_2O with trace amounts of N_2 and NO from gas chromatographic analysis [19]. Additionally, using infrared analysis, the decomposition products were mostly N_2O with some NO_2. NO_2 and NO were considered a further decomposition of nitric and nitrous acid. Schoppelrei and Brill employed FT-IR and observed the formation of N_2, NO, and NO_2 when "flash heating" within Argon at 3.5 MPa. They hypothesize that the NO and NO_2 are secondary formations from HNO_2 and HNO_3 contained in the mixture [27]. Using IR spectroscopy, Rafeev and Rubstov thermally decomposed HAN into NO_2, NO, N_2O, and H_2O within a temperature range of 84.8°C to 120.9°C [13]. The products of the aforementioned decomposition experiments are summarized below in Table 1.

Table 1: Summarized decomposition products from previous literature

		Decomposition Products						
Temperature (˚C)	Pressure	HNO_3	HNO_2	N_2O	NO	NO_2	N_2	H_2O
200	1 atm	x		x	x	x		
180	1 Mbar			x	x	x		
174	1 atm			x	x	x		
129-139	N/A			x	x	x	x	x
"flash heating"	3.5 Mpa				x	x	x	
84.8 - 120.9	N/A			x	x	x		x

The use of a catalyst reduces the temperature at which decomposition occurs for a given concentration. Similarly, the use of a catalyst reduces the HAN concentration needed for decomposition to occur (for a given temperature) [4], [6], [7]. Therefore, using a catalyst makes the decomposition of HAN possible at room temperatures, and no change to decomposition products is reported [4]. Amrousse et al. also concludes that the use of a catalyst allows for the decomposition of HAN-water at lower temperatures [7]. Even though no changes in decomposition products are reported, it is still unclear whether the presence of a catalyst alters the resultant gaseous species.

Diagnostic Determination

A variety of diagnostic tools have been used to determine the decomposition products of HAN and HAN-based propellants from either thermal or catalytic decomposition. The decomposition products from HAN, as seen above, are predominantly determined from FT-IR and Raman spectroscopy. The use of mass spectroscopy or a similar system for filtering and detecting mass to charge ratios has been used for determining decomposition products as well [4], [8], [28]. Both FT-IR and Raman spectroscopy are powerful tools and have detected the intermediary

decomposition products [8], [14]. However, due to the nature of spectroscopy, the intensity of the signal is a function of gaseous concentration as seen by the Beer-Lambert law below [29],

$$\mathrm{A} = \log_{10}\left(\frac{I_o}{I}\right) = \varepsilon(\tilde{\nu})\, c\, l \tag{1}$$

where A is the absorbance, c is the concentration of the sample with length l, and $\varepsilon(\tilde{\nu})$ is the molar absorbance coefficient. Absorbance is also defined as the log of incident intensity I_o divided by irradiated intensity I. The density of gas in a vacuum chamber is in very low concentration, and therefore, diagnostic tools that operate in low pressure environments must be employed. Therefore, a Residual Gas Analyzer (RGA) was chosen for the sampling of gaseous species under vacuum conditions.

CHAPTER III

DIAGNOSTICS

How RGAs Work

A residual gas analyzer, as seen in Figure 4, works similarly to a mass spectrometer. Residual gases are ionized to form positively charged particles, filtered with respect to their mass-to-charge ratio, and collected to determine ion current. The ion current is used to resolve partial pressure of a gas. The ions are created by high energy (up to 70 eV) electron collisions [30]. These electrons impact with enough energy to surpass the ionization energy of most molecules, and therefore, remove an electron in the process.

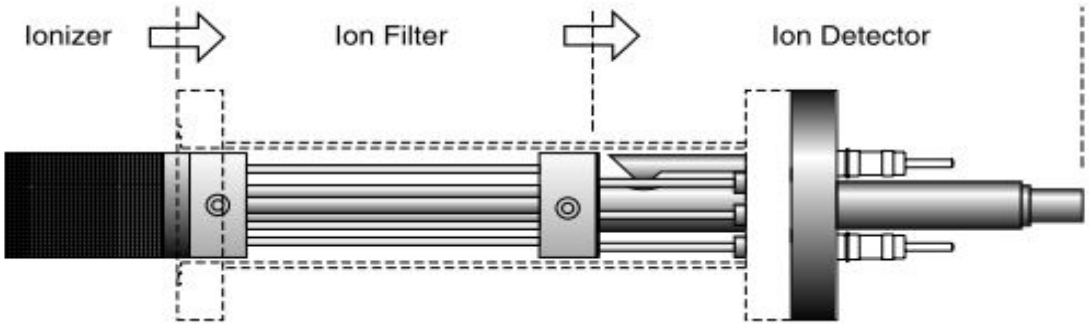

Figure 4: RGA probe diagram [30]

The quadrupole mass filter is used to selectively determine which ions are measured at any given time. Four cylindrical electrodes establish the quadrupole field: two opposing electrodes are connected to positive DC voltage, and the other two opposing electrodes are biased with negative DC voltage. Both the positive and negative DC voltages have a superimposed out-of-phase RF voltage applied. A stable ion trajectory is created for a specific mass to charge ratio (M/Q) as the RF and DC voltages are 'swept' through changing amplitudes [30]. The partial pressure of a gas that has been filtered is calculated based on the incident ion current that the Faraday cup directly

measures [30]. It is important to note that the atomic mass unit (AMU) is used to describe the mass of individual ions where the ratio is equal to the atomic mass (M) for a charge (Q) of one [30]. For doubly ionized particles, the observed AMU value would be half of the expected AMU value, due to a mass (M) divided by a charge (Q) of two.

Interpreting RGA Data

The mass spectra resulting from an RGA sweep needs to be interpreted to obtain the identity and partial pressures of the various gases. Peaks on the mass spectrum can be a result of more than one gas. For example, 28 AMU could be N_2 or CO. Therefore, it is important to acknowledge recent uses of the facility and what residual gases may be present from previous work. An air leak in the system can lead to erroneous results due to an excess of nitrogen, oxygen, carbon dioxide, etc. Also, determining what gases are unlikely to be in the vacuum chamber, based on elements introduced into the system, will help narrow the possible peaks that are present. Understanding fragmentation profiles help define peaks in the mass spectra as they could be solely created by, or simply increased by, the fragmentation of residual gases [30].

The addition of large amounts of gas into a system can have a significant effect on the results of the RGA. The introduction of a gas into a vacuum system will affectively displace existing gas within the chamber. The RGA will detect both the new gas and the existing gas; however, the concentration and partial pressure of the existing gas will decrease, when compared to the overall pressure. The amount of gas in the system does not change when a new gas is added, but the overall increase in pressure needs to be taken into account when analyzing partial pressure data.

In the case where the RGA is separated from the vacuum chamber by a needle valve and resides in a lower pressure environment using a differential pumping system, the effects of a

sudden rise in pressure can result in an unexpected change of partial pressures within the RGA system. When the RGA samples a gas through a needle valve from a higher pressure environment, the flow through the needle valve can become choked. The mass flow rate through the choked valve is a function of the reservoir pressure, or the pressure of the chamber being sampled. When the pressure in the chamber quickly increases, the gas within the needle valve tubing is suddenly pushed into the ionizer of the probe, resulting in an increase of that gas, even though no more of the gas was added to the system.

Fragmentation

Due to the ionization process, more than one ion can be created from a single residual gas molecule as a result of electron impact. A molecule can be dissociated into other molecules or into its molecular components from the high energy electrons, resulting in multiple ionized fragments. This phenomenon is known as fragmentation. The ions created as a result of fragmentation add to the total mass spectrum. Many molecules has been studied and their fragmentation profiles are well known. The Stanford Research System's RGA computer software has a library of fragmentation profiles, and those profiles were used for analysis of experimentally gathered RGA data.

Water is commonly present in vacuum chambers, and therefore RGA scans will see this as AMU 18. Figure 5 shows the fragmentation profile for water, which identifies fragments of ionized water to be AMU 17 and 16, or ionized OH and O, respectively.

The fragmentation profile is further described below in Table *2*. All five AMU values are provided by the RGA fragmentation library, and can be seen in Figure 5, however, AMU 19 and 20 are in such low percentages that their presence is ignored.

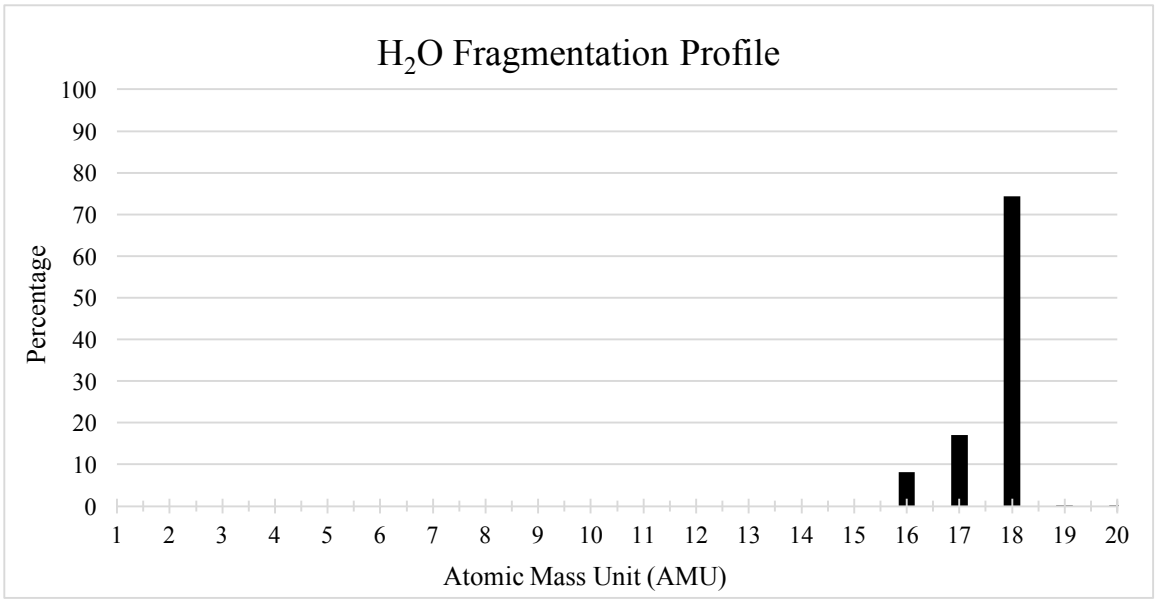

Figure 5: Fragmentation profile of H_2O, AMU 18

Table 2: Fragmentation profile of H_2O, AMU 18

Mass	**16**	**17**	**18**	**19**	**20**
%	8.18452	17.1131	74.4048	0.0744048	0.223214

In addition to the fragmentation profile, hydrogen is also present in RGA scans as a result of water fragmentation. It is believed that the hydrogen molecule is produced by further fragmentation of the OH and H_2O at 70 eV. According to the National Institute of Standards and Technology (NIST) database, H_2 ions are formed from H_2O at 20.7 eV ± 0.4 eV, in addition to molecular oxygen [31]. A hydrogen molecule has less mass then molecular oxygen, and assuming they part from the molecule with equal energies, the hydrogen will have a higher velocity to maintain conservation of momentum. Therefore, hydrogen is much more difficult to pump out of a vacuum system and will appear in higher quantities. Figure shows an RGA analog scan at various electron impact energies given in eV, and mass peaks at AMU 2, 16, 17, and 18.

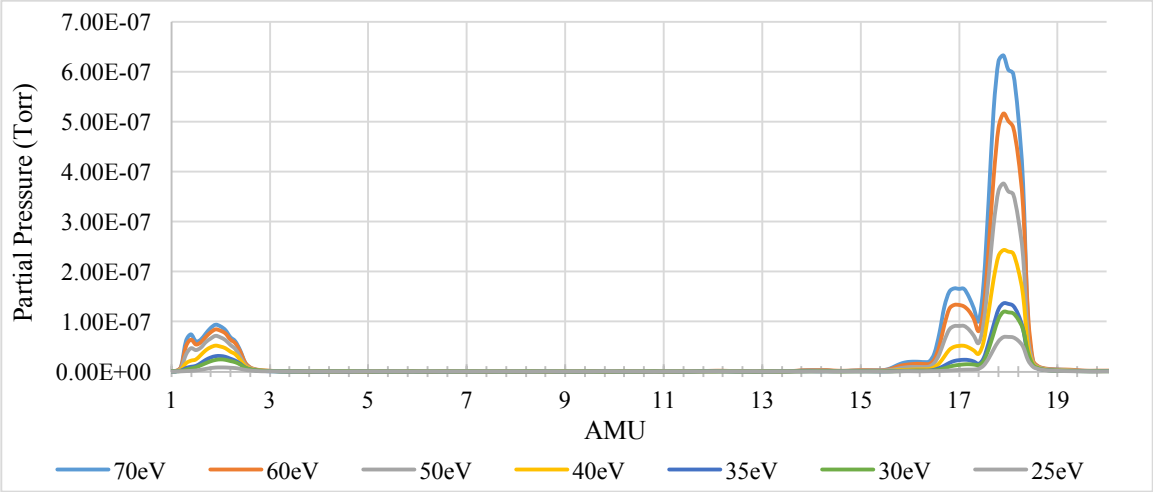

Figure 6: Fragmentation profile of H_2O at various electron impact energies

The sensitivity of the RGA system is significantly reduced when the electron impact energy is reduced. The quadrupole mass filter has less of an effect on particles of lower energy than of high energy. In order to maximize the sensitivity of the RGA system, the RGA was set at 70 eV electron impact energy. It is preferable to have high fragmentation due to the high electron impact energy than potentially not detecting particles that are present in the system.

The fragmentation profiles of N_2O, NO, and NO_2 were also investigated. These gases are present in the experimental results of this paper, as well as in previous research. Therefore, it is necessary to understand how these gases interact with the RGA filament, so more accurate conclusions can be drawn. Tables 3, 4, and 5, and Figures 7, 8, and 9, show the fragmentation profiles given by the RGA fragmentation library.

Table 3: Fragmentation profile of N_2O, AMU 44

Mass	**14**	**15**	**16**	**28**	**29**	**30**	**31**	**44**	**45**	**46**
%	8.065	0.062	3.102	6.824	0.062	19.231	0.062	62.035	0.434	0.124

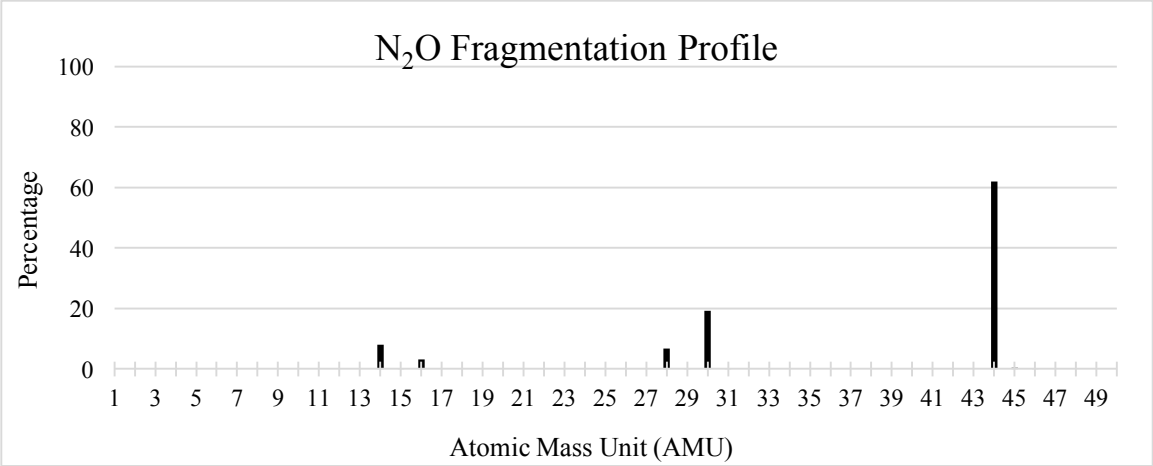

Figure 7: Fragmentation profile of N_2O, AMU 44

Table 4: Fragmentation profile of NO, AMU 30

Mass	**14**	**15**	**16**	**30**	**31**	**32**
%	7.073	2.210	1.768	88.417	0.354	0.018

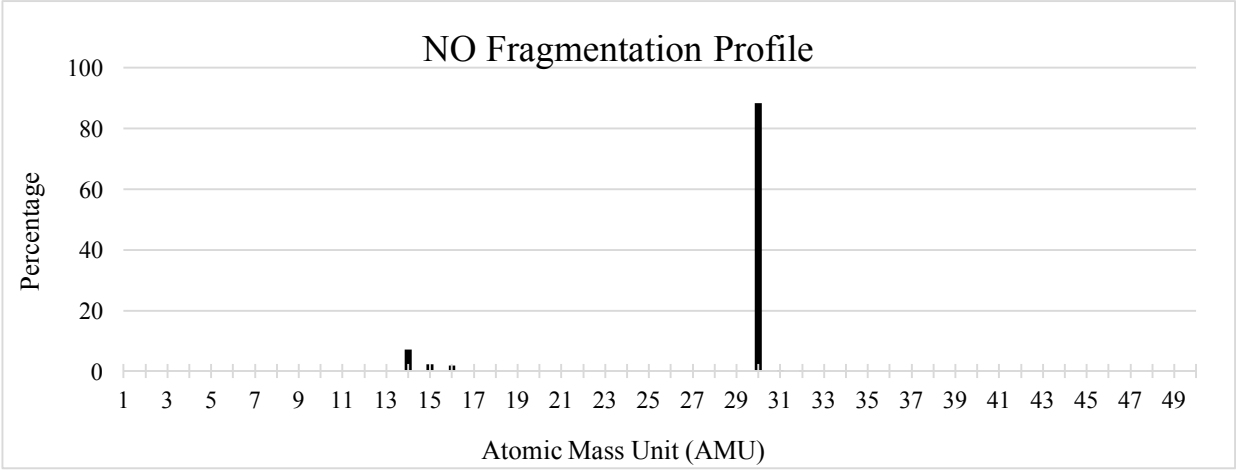

Figure 8: Fragmentation profile of NO, AMU 30

Table 5: Fragmentation profile of NO_2, AMU 46

Mass	**14**	**16**	**30**	**31**	**46**
%	5.903	12.987	59.032	0.236	21.842

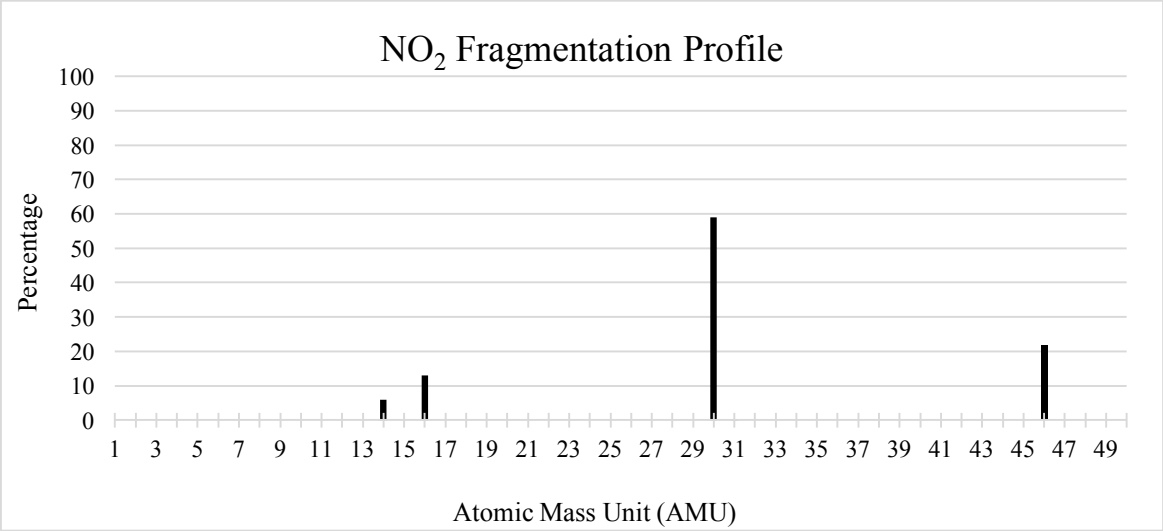

Figure 9: Fragmentation profile of NO_2, AMU 46

When N_2O is ionized, the RGA spectra will appear to have a significant amount of AMU 30, and a slight amount of AMU 28, 14, and 16. Of significance are AMU 30 and 28 because they are the mass values of NO, and N_2, respectively. The majority of N_2O present in the system will register as such, AMU 44. Similarly, when NO is ionized, it will show up as the majority AMU 30 with a small amount of atomic nitrogen at AMU 14. However, when NO_2 is ionized, the spectra will register NO at AMU 30 as the majority and not NO_2 at AMU 46. NO_2 presents itself as nearly a third of what is truly present in the system. Understanding the fragmentation of these gases will help in the analysis of RGA data as well as in the determination of gases produced from the decomposition of HAN.

CHAPTER IV

VACUUM CHAMBER AND EXPERIMENTAL SETUP

Vacuum Chamber System

All research was performed at the Aerospace Laboratory for Plasma Experiments at Western Michigan University using a 2-ft-long by 2-ft-diameter 316 stainless steel vacuum chamber with an ultimate base pressure of 2.5E-6 Torr. The vacuum chamber has two doors, one on each end, and various 2.75-in and 4.00-in ConFlat feedthrough flanges. A diagram of the chamber can be seen in Figure . The pumping system consists of a Varian TriScroll 600 dry scroll pump shown in yellow, with an ultimate pressure of about 7.6E-3 Torr.

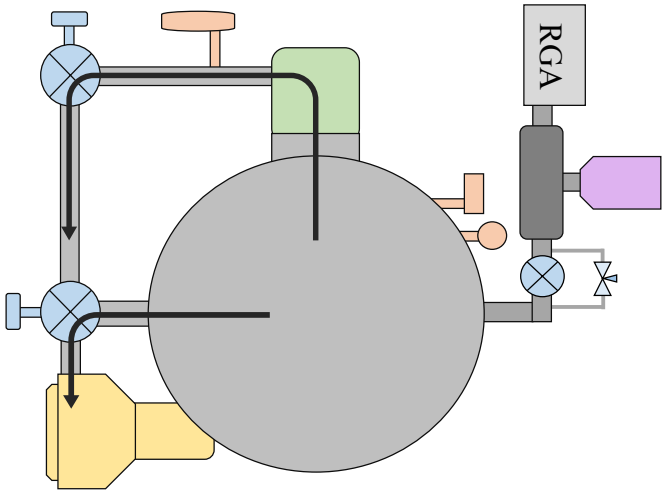

Figure 10: Vacuum chamber diagram

This pump is fitted with a nitrogen bearing purge which allows a flow of nitrogen into the axial bearings of the pump, thus helping prevent the buildup of particulates and moisture. In addition to the purge, the pump also utilizes an automatic gas ballast, which also helps prevent the buildup of particulates and moisture. However, the ballast port provides a conduit for air to migrate back into the vacuum chamber. This pump design flaw allows for air to leak into the chamber, while still

maintaining specified base pressure. The roughing pump connects directly to the chamber and serves as the backing pump for the top mounted Varian Turbo-V 550 l/m, shown in green. There are three pressures gauges on the vacuum chamber, shown in orange: 1. A WorkerBee™ convection gauge for the chamber itself; 2. a WorkerBee™ convection gauge on the exhaust of the turbo pump; and 3. a Hornet™ ion gauge on the chamber for pressures below 1.00E-3 Torr.

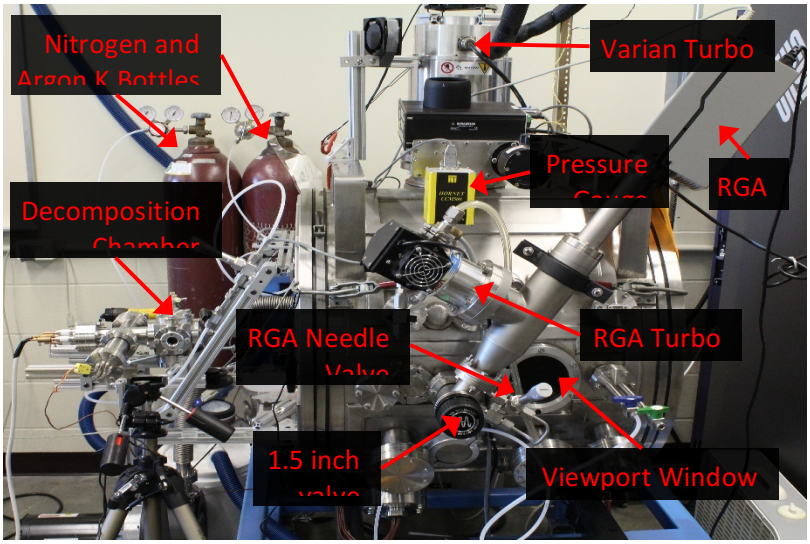

Figure 11: Vacuum chamber system

The Stanford Research Systems Residual Gas Analyzer, shown in Figure 10 as well as Figure 11, is connected to the chamber via a differential pumping system. The differential pumping system, consisting of a Varian Turbo-V 70 l/m Macro Torr turbo pump and shown in purple, is backed by an oil vane roughing pump, which is not shown. This added pumping system allows for gas sampling from the vacuum chamber through a needle valve when pressures are higher than the RGA is capable of handling. The RGA cannot operate in pressures above 1E-4 Torr. When the turbopump is operating and the vacuum chamber is at or below 1E-4 Torr, the 1.5-in valve that resides between the chamber and the differential pumping system must be open to allow gasses to reach the RGA. If the larger valve is not used, the lack of differential pressure will prevent gasses

from reaching the RGA, whereas with higher chamber pressures, the needle valve must be used to ensure the pressure surrounding the RGA filament is below 1E-4 Torr.

Experimental Setup

Three different experimental setups were used for the decomposition of HAN, all of which utilize the vacuum chamber system explained above. Experimental Setups 1 and 1B are attached to the door on the left side of the vacuum chamber as seen in Figure 11 and utilize the decomposition chamber (DC). Experimental Setup 2 does not use the DC; it only uses the vacuum chamber. The DC is unable to achieve the same low pressure as the vacuum chamber when using the turbo pump due to conduction losses through the tube that connects the vacuum chamber and the DC. Therefore, experiments that are designed for very high vacuum are done inside the vacuum chamber, and thus use Experimental Setup 2. It should also be reiterated that the roughing pump allows for a small amount of air to leak into the vacuum chamber. This air leak is noticeable when using the RGA and results in undesirable partial pressures of nitrogen and oxygen measured by the RGA.

Decomposition Chamber: Experimental Setups 1 and 1B

As shown below in Figure 12, a separate volume was used as a decomposition chamber, instead of the vacuum chamber itself. The advantage to using a smaller, separate volume, is the ability to control the experimental conditions and experiment turnaround time. The DC is built using a 6-way 2.75-in ConFlat cube and a 4-way 2.75-in ConFlat cross.

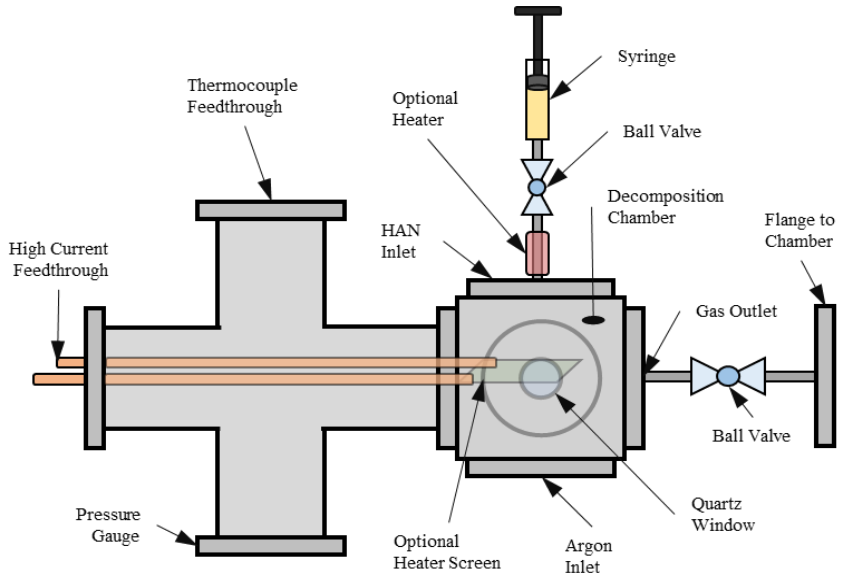

Figure 12: Decomposition chamber diagram

At the bottom of the cube is a 1/4-in Swagelok inlet port for backfilling with Argon. This port also serves as a drainage port for cleaning the DC. Attached to the cross is a type-K thermocouple feedthrough, a high current feedthrough, and a WorkerBee^{TM} convection gauge. A quartz window resides on two opposite sides of the cube. The windows are used for visual inspection of the heater placement, as well as documenting the changes to HAN throughout the experiment. The cube is connected to the vacuum chamber using a set of 2.75-in ConFlat to 1/4-in Swagelok flanges. The flanges are connected using 1/4-in stainless steel tubing with an inner diameter of 0.185-in and a Swagelok ball valve. This valve is used to isolate the DC from the pumping system allowing for a quick evacuation after modifications and maintenance. The top of the cube is reserved for a liquid feedthrough flange. Two different liquid feedthrough flanges were built, both using a 2.75-in ConFlat flange and a 304 stainless steel tube. The tubes for both feedthroughs used Aron Ceramic D ceramic adhesive by Toagoseo Co., LDT to physically secure the tube within the feedthrough, and Vacseal Resin vacuum sealant from SPI Supplies was used around the base of the tube to provide an air-tight seal. In addition, a ball valve is attached to the tube on the atmospheric side to

allow for the attachment and removal of a syringe without exposing the DC to atmosphere. The valve is also used to introduce the syringe contents into the DC when required. Figure 13 shows the constructed decomposition chamber.

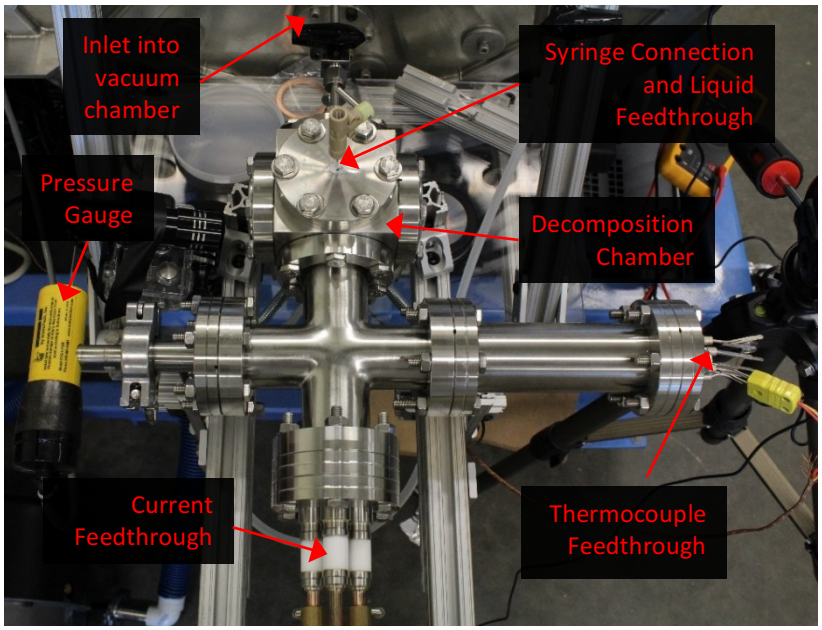

Figure 13: Decomposition chamber

Experimental Setup 1: Liquid Feedthrough with Heater Screen

Experimental Setup 1 utilizes the DC with the optional heater screen, and the liquid feedthrough. The heater used inside the DC uses a nickel-chromium (nichrome) wire mesh as the resistive heating element. The mesh consists of 0.020-in-diameter wire with 0.043-in-spacing. This material was chosen for its high resistance to oxidation, as well as its high melting temperature, and the mesh design was chosen for high surface contact area. The wire mesh was cut to increase the resistive path while maintaining a high level of surface area.

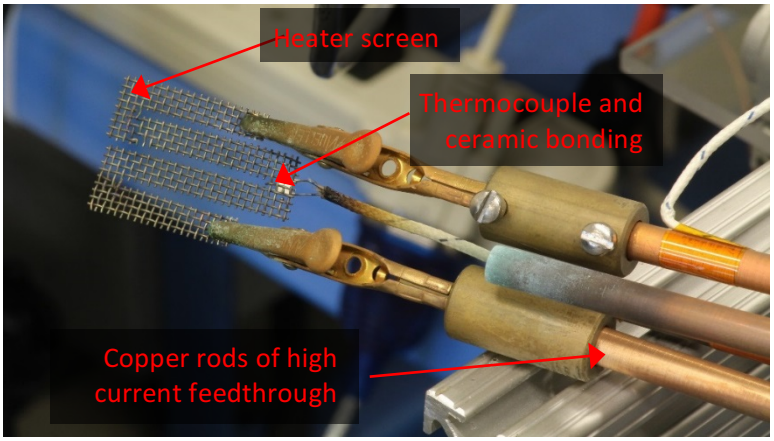

Figure 14: Heater assembly consisting of a nicrome wire mesh as the heating element, copper alligator clips, and copper high current feedthrough rods

The heater, as seen in Figure 14, is supported and electrically connected to the high current copper feedthrough bars using copper alligator clips and brass set screw butt splices. The heater is positioned between the two quartz windows, directly beneath the liquid feedthrough. Temperature of the heater is measured using a type-K thermocouple. The thermocouple is physically secured to, and electrically isolated from the screen using alumina ceramic paste.

The liquid feedthrough utilized for this experimental setup is shown below in Figure 15. The assembly consists of a 0.0625-in-OD, 0.045-in-ID, 2-in-long, stainless steel tube that extends a 1/4-in past the inner surface of the flange. The setup allows for the dropping of HAN onto the heater screen while under vacuum conditions. This liquid feedthrough flange was designed to minimize the volume from the syringe to the DC. The smaller the combined volume of the tube and ball valve, the less HAN is needed to form droplets on the vacuum side of the tube.

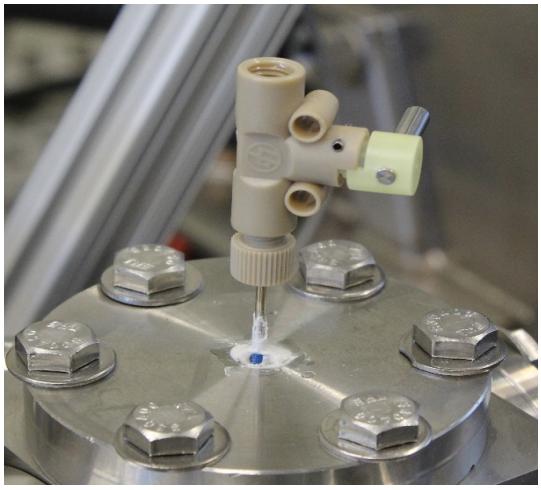

Figure 15: Liquid feedthrough for experimental setup 1

Figure 16 shows the installed heater screen inside the DC. The copper alligator clips from the left side in the image support the heater screen, and the flange that connects the DC to the vacuum chamber is on the right side of the image. Present on the heater screen are droplets of HAN under atmospheric conditions and no heat.

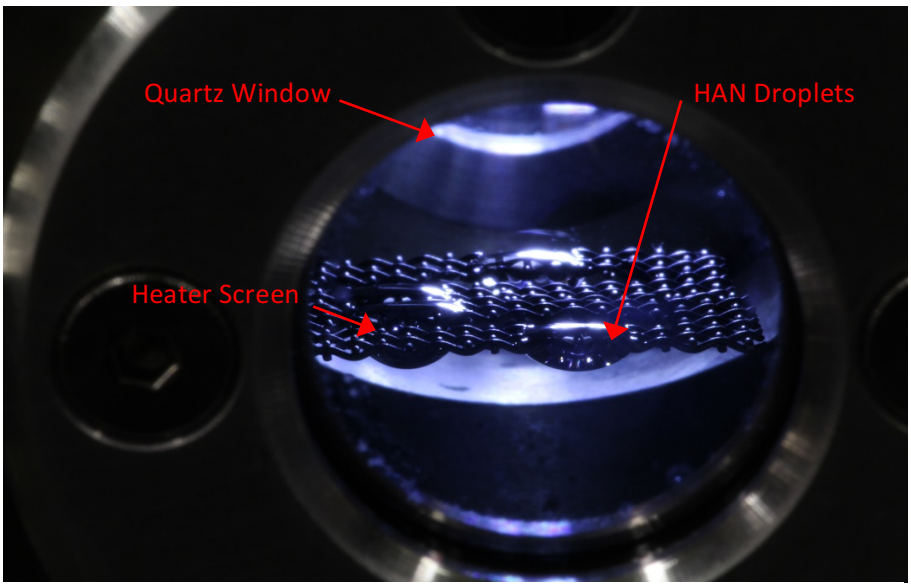

Figure 16: Heater screen in DC with HAN droplets

Experimental Setup 1B: Liquid Feedthrough with Tube Heater

Experimental Setup 1B differs from Experimental Setup 1 by an external heater on the liquid feedthrough. The heater is wrapped around the stainless steel tube used for introducing liquid from the syringe into the DC. The 0.0563-in-OD, 0.040-in-ID, 2-in long tube is secured in a modified 2.75-in ConFlat flange. The flange modification allows for more of the tube to be exposed, permitting a greater surface area of the tube to be heated. The heater itself is tantalum wire, which is tightly wound around an 1/8-in-OD, 1/16-in-ID ceramic tube, and potted with ceramic paste. The ceramic tube is able to slide over the steel tube and rotate freely to prevent stress on the heater wire and ceramic paste. A type-K thermocouple is attached to the stainless steel tube just below the heater using Aron Ceramic D ceramic adhesive. There is no heater employed on the inside of the decomposition chamber for this experimental setup. However, the internal heater is still present.

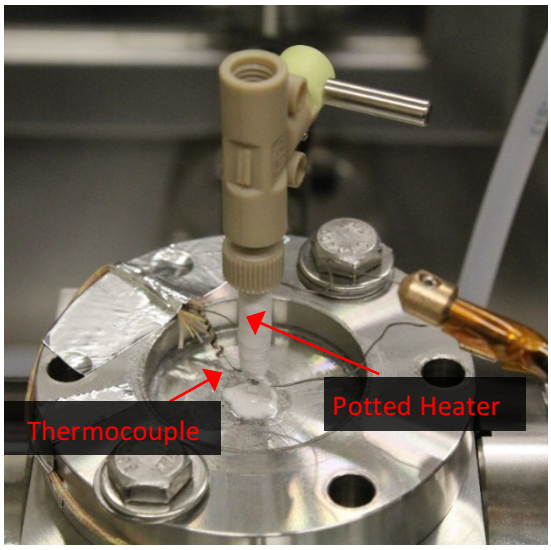

Figure 17: Liquid feedthrough with heater and thermocouple on stainless steel tube

Experimental Setup 2: Vacuum Chamber Decomposition Setup

The vacuum chamber decomposition setup utilizes the vacuum chamber itself rather than the DC setups. In this configuration, the roughing pump and turbopump, pump directly on the volume of this chamber. The RGA is also directly connected to the volume where the heater resides, rather than separated by a 6-in-long, 1/4-in-OD stainless steel tube. The primary purpose of this setup is to reduce the pressure to which the HAN sample is exposed below ~5.0E-3 Torr. With the turbopump operating, and no HAN present, the vacuum chamber can achieve a pressure as low as ~2.5E-6 Torr, whereas the DC, at the same time, will achieve a pressure only as low as ~5.0E-3 Torr.

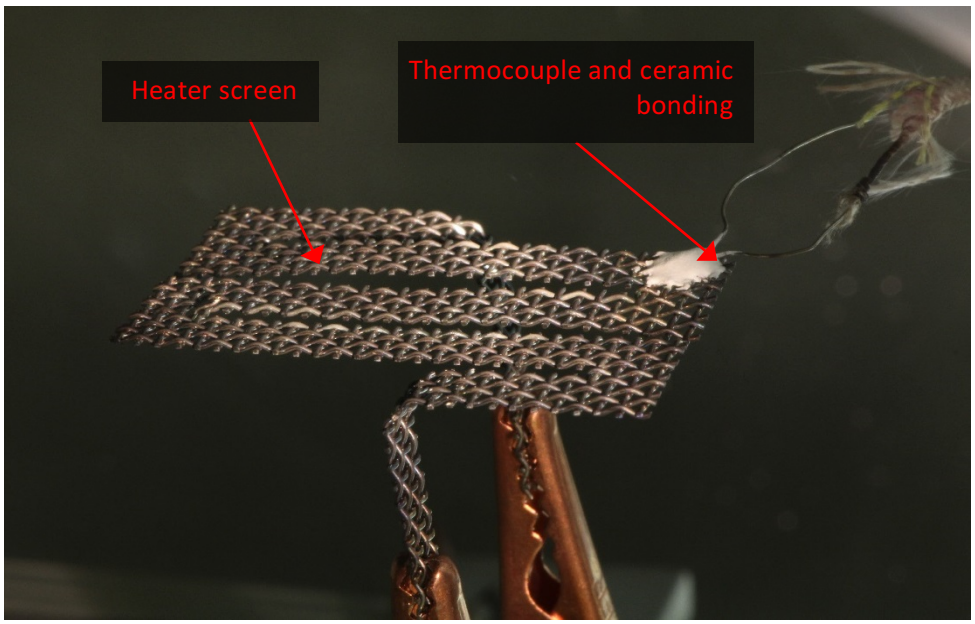

Figure 18: Heater screen assembly in vacuum chamber consisting of nicrome wire mesh, type-K thermocouple, and copper alligator clips

The heater screen seen in Figure 18 is held and electrically connected using two copper alligator clips. These alligator clips connect to the high current feedthrough via high current fiberglass insulated wire. The temperature of the screen is measured using a type-K thermocouple which is

physically connected to, and electrically isolated from, the heater screen with alumina ceramic paste. The heater assembly is positioned in front of the vacuum chamber's side view port window for visual observation. In this configuration there is no method to introduce HAN onto the screen once the chamber has been sealed. For all experiments utilizing this setup, the HAN is applied to the screen prior to closing and evacuating the chamber. One other disadvantage is that the RGA cannot sample the vacuum chamber until the pressure has been lowered to ~5.0E-1 Torr due to the pressure that would result inside the RGA. Therefore, any decomposition that takes place before this pressure is achieved, cannot be detected.

Data Acquisition System

The data acquisition system (DAQ) is used to monitor and record conditions within the decomposition chamber and vacuum chamber. The DAQ is a NI c-DAQ 9178 Compact DAQ module unit with an NI 9211 TC ± 80 mV DIFF (thermocouple reader) and NI 9215 AI ± 10 V DIFF SSH modular units (analog voltage input). The pressure sensor control box outputs a 0-10 V signal relating to pressure. The pressure voltage is read by the AI module and LabVIEW converts the voltage to a pressure value. The thermocouple data is read in a similar manner. The DAQ is controlled by a LabVIEW VI that also records data.

CHAPTER V

EXPERIMENTAL RESULTS

Since all experiments were performed under vacuum, the concentration of HAN, which is known prior to testing (24% wt. in Water, Sigma Aldrich), becomes unknown once exposed to vacuum. The reduced pressure causes water to evaporate from the HAN solution and therefore increases the concentration. From what is known about HAN, water acts as a stabilizing agent, keeping it from decomposing. The induction period - the time it takes for decomposition to occur, is dependent on the temperature and pressure. The lower the pressure within the vacuum chamber or the decomposition chamber, the more water that has been removed. All data were collected using the RGA, alongside thermocouple and pressure readings. The RGA gives the amount of gas present in terms of partial pressure. Therefore, all quantitative data on the amount of gas present as a result of decomposition are given as relative partial pressure. The effects of fragmentation will be discussed alongside the results. The resultant gaseous species from HAN decomposition under vacuum conditions are observed to be predominantly N_2O and NO, with trace amounts of NO_2.

HAN Exposed to Vacuum Conditions

When HAN is exposed to vacuum conditions, decomposition occurs, even in the absence of added heat. HAN at room temperature and low pressure, produces nitrous oxide, N_2O. Water could also be a decomposition product; however, due to the presence of water evaporation from the HAN-water solution being investigated, the amount of water produced as a result of HAN decomposition cannot be determined from this experiment. Figure 19 shows an RGA scan of partial pressure as a function of elapsed time for various gaseous species.

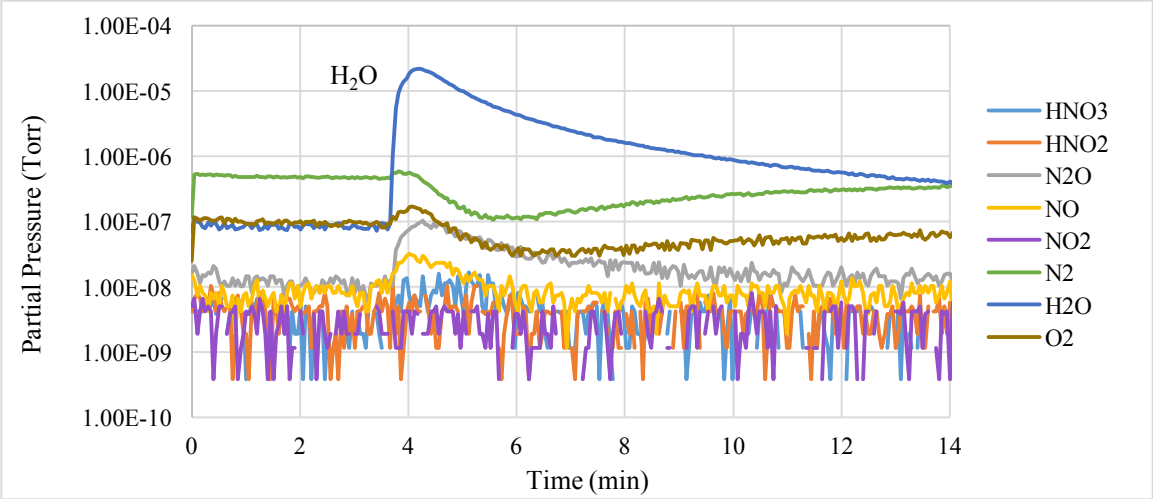

Figure 19: HAN exposed to vacuum through a non-heated tube

Experimental Setup 1, which utilizes the decomposition chamber, was used to obtain the results seen above in Figure 19. HAN was introduced into the DC via the liquid inlet feedthrough seen in Figure 15. The heater screen was present in the experimental setup; however, it was not used. The thermocouple reading on the heater screen was used to determine the temperature on the inside of the DC. Before the valve to the needle was opened, the DC was initially at 21˚C and 9.70E-3 Torr. The opening of the valve allowed 0.07 mL of HAN to be exposed to vacuum. The water that is in solution with HAN starts evaporating as soon as it is exposed to vacuum. Nitrogen and oxygen also increase, which is likely from the small amount of air that is trapped within the ball valve used to isolate the DC from atmosphere. Nitrogen could be a decomposition product, but it cannot be differentiated from the existing nitrogen in this experiment. N_2O formation occurs when HAN is exposed to vacuum, and does not require any added heat to occur. The presence of NO was also detected, but it is unclear whether or not it is a result of decomposition since N_2O fragments into ~20% NO, according to the RGA fragmentation library. The RGA scan also shows a small increase in HNO_3. These trace amounts suggest that HNO_3 is being formed as a result of HAN exposure to vacuum.

To help confirm the decomposition of HAN under vacuum conditions, as well as better understand the effects of fragmentation, HAN was introduced into the DC while at vacuum. Figure 20 was generated by plotting the normalized maximum partial pressure of N_2O and NO. The values of N_2O and NO are normalized by the amount of H_2O present to account for any variation in the amounts injected HAN. For each experiment, the temperature remained at 21˚C ±1˚C, and the amount of HAN was controlled by filling a syringe to 0.07 mL. The pressure of the DC was achieved by allowing the DC to be evacuated until the desired pressure was met. The differences in pressure were a result of the amount of water in the DC from the previous experiment. N_2O and NO levels returned to background levels before the desired DC pressure was achieved. The products, N_2O and NO, are plotted as partial pressure on the y-axis, and initial DC pressure on the x-axis.

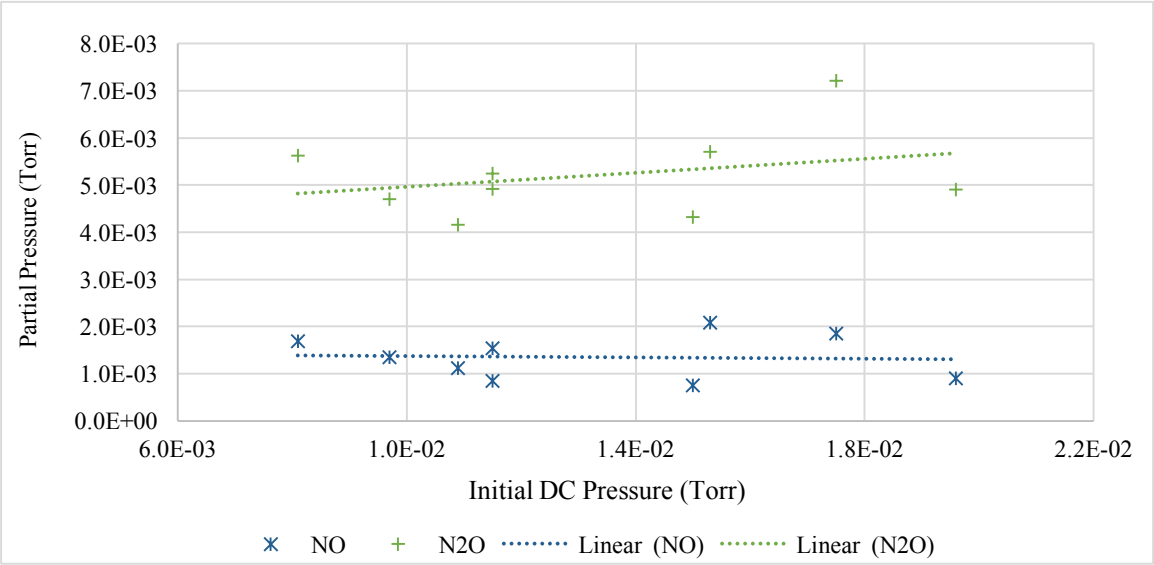

Figure 20: HAN exposed to DC at vacuum

There were eight experiments conducted over a pressure range from 8.10E-3 to 2.0E-2 Torr. During each experiment, the pressure increased to approximately 4 Torr when the HAN was injected into the DC. This experiment confirms that N_2O is produced from the exposure of HAN

to vacuum conditions. The fragmentation profile of N_2O suggests that it fragments into ~20% NO. In figure 20, NO averages 26% of N_2O, and is therefore believed to be largely a result of fragmentation. HNO_3 was also present on the RGA scans in trace amounts. No error analysis was conducted on the data in Figure 20.

HAN Heated under Vacuum Conditions

Using Experimental Setup 1, HAN was dripped from the liquid feedthrough onto an unheated screen; the screen was later heated. Figure 21 shows that the HAN injection occurred just after the 9.5 minute mark, and the pressure in the DC rose to 4.6 Torr before the products were pumped from the DC. Before the HAN injection, the initial pressure of the DC was 2.3E-2 Torr, and the initial temperature of the screen was 23°C. N_2O, NO, and NO_2 are formed as a result. The majority of H_2O is likely attributed to the water in the HAN-water solution.

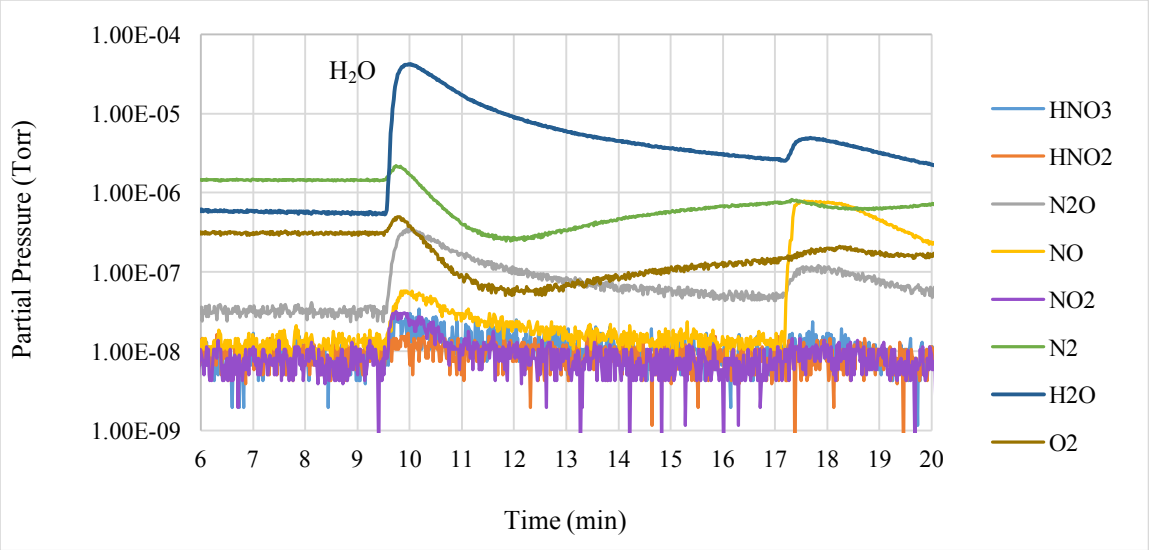

Figure 21: HAN dripped onto room temperature heater screen, and then heated

Any H_2O formation as a result of HAN decomposition cannot be differentiated from the H_2O in the injected solution in this experiment. The increase in N_2 and O_2 is likely a result of the ball valve being opened with trace amounts of air in the valve. A small of amount of air enters the ball valve

when the syringe is removed and re-attached. However, the formation of N_2 is possible and requires further investigation. Similar to the previous section, N_2O is a clear resultant gas. Also present is NO and trace amounts of NO_2. NO could be the result of N_2O and NO_2 fragmentation; however, NO, as a decomposition product, cannot be ruled out. Additionally, the formation of NO_2 has not been seen in other experiments where HAN is solely exposed to vacuum conditions. The presence of HNO_3 is also seen in similar partial pressures to NO_2.

Approximately 8 minutes after dropping HAN onto the heater screen (indicated after 17 minutes in Figure 21), it was turned on, and the temperature rose from 23˚C to 620˚C in 68 seconds. It took 21 seconds to reach 500°C and 38 seconds to reach 600°C. The last 20°C took 30 seconds. The most prominent gas produced was NO, followed by N_2O. The increase in water that resulted from an increase in temperature is either caused by the formation of H_2O from the decomposition process or from the evaporation of the remaining water in the HAN solution. Also present as a result of flash heating to 620˚C are trace amounts of HNO_3 and NO_2. It is understood that NO_2, as a result of the RGA ionizer, becomes 59.0% NO and 21.8% NO_2; therefore, the amount of NO measured by the RGA is likely increased from NO_2 and N_2O fragmentation. However, the total amount of NO produced is not a result of fragmentation. Fragmentation of N_2O and NO_2 increase the partial pressure of NO by 2.3E-8 and 8.5E-9 Torr, respectively. The NO partial pressure of 3.15E-8 Torr from fragmentation is a small fraction of the total NO partial pressure, 7.7E-7 Torr. Therefore NO is a clear decomposition product. The formation of HNO_3 was observed during heating, but the initial introduction of HAN prior to heating resulted in more HNO_3.

In order to better understand how temperature and pressure affects HAN decomposition, experimental setup 1B was employed to run 38 experiments over a wide range of temperatures and pressures. Before each experiment, HAN solution was drawn into a syringe and all air bubbles

were removed, leaving 0.07 mL of HAN solution. All partial pressure data from the 38 experiments are from the peak measured value of each gas during the test. The data are normalized using the partial pressure of H_2O to account for the variation in the amount of HAN solution actually injected during each experiment. Figure 22 shows the partial pressure of N_2O and NO per each experiment as a function of the maximum tube temperature. The reason for using the maximum temperature is described in the following paragraph. Figure 22 does not differentiate between the initial pressures of the DC prior to opening the valve. However, the experiments spanned pressures from 6.0E-3 Torr to 4 Torr.

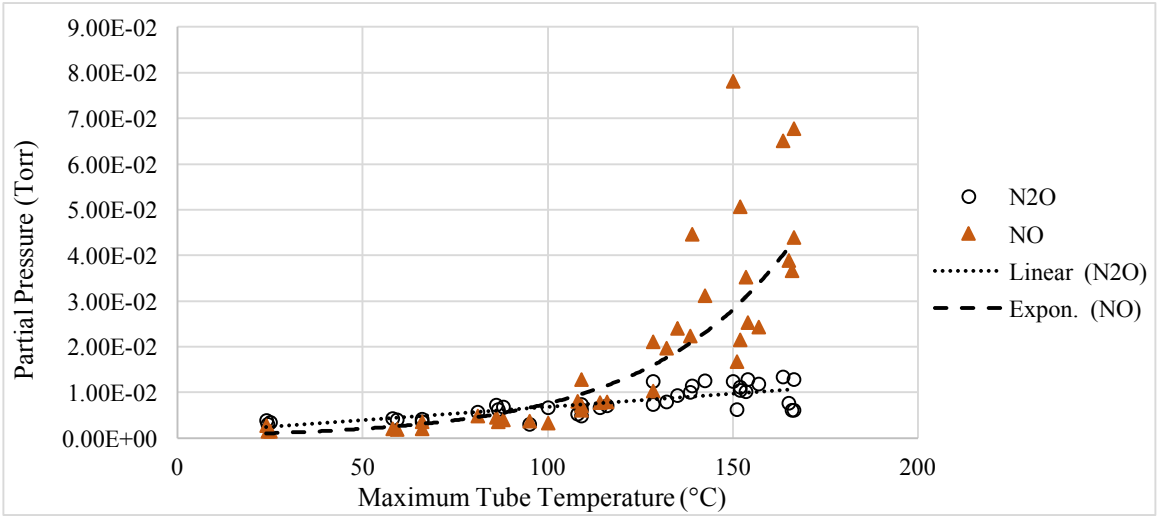

Figure 22: HAN exposed to varying levels of vacuum through a tube at varying temperatures

Seven temperature set points for the inlet tube were selected, ranging from 25°C to approximately 142°C. Each temperature set point was the tube temperature prior to the opening of the valve. Opening the valve exposed the HAN solution to vacuum, thus pulling it through the tube into the DC. The temperature profile of the inlet tube varied in three distinct ways: (1) initial exothermic reaction, (2) initial cooling followed by a slow exothermic reaction, and (3) initial cooling followed by a fast exothermic reaction. The exothermic reactions raised the temperature of the inlet tube. This increase in temperature is believed to have affect the amount of NO produced; and therefore,

the maximum tube temperature was used in place of the set tube temperature in Figure 22. This resulted in a more accurate graph relating NO production and temperature. As the temperature set points increased, the production of NO became more prominent. Alternatively, the amount of N_2O measured remained relatively linear as the temperature set points increased.

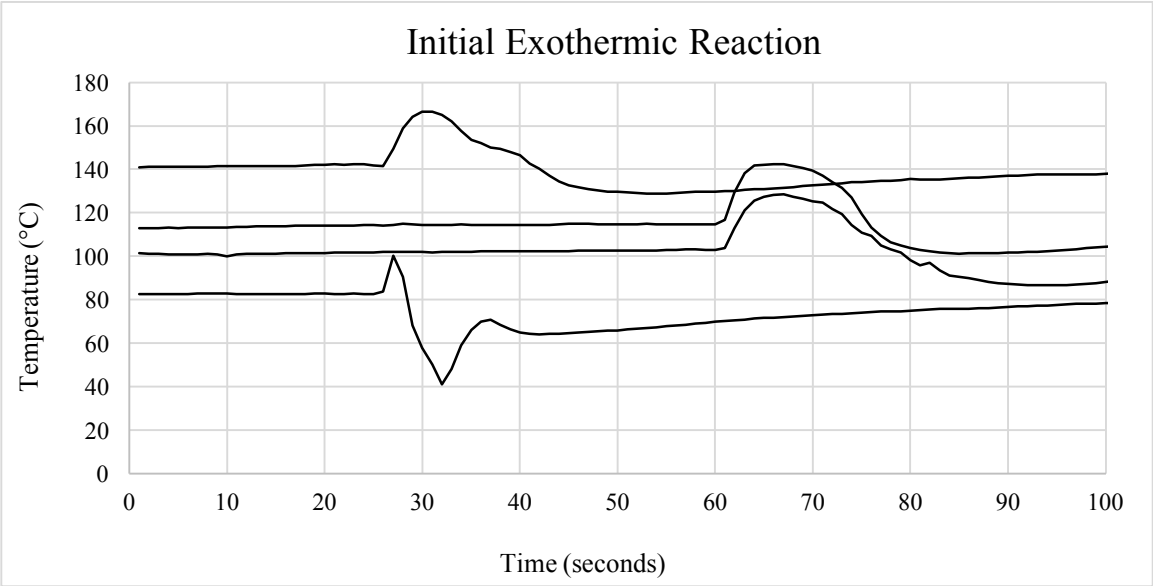

Figure 23: Temperature profiles of liquid feedthrough, 'initial exothermic reaction'

From the thermocouple placed on the stainless steel tube, a temperature profile was recorded for each test during the experiment. From all 38 tests, three distinct temperature profiles became apparent. The liquid feedthrough tube would often experience an immediate temperature increase when HAN was exposed to the heated tube under vacuum. This temperature profile is denoted as 'initial exothermic reaction' and can be seen in Figure 23. Some tests resulted in an initial cooling affect, followed by a rise in temperature, where the temperature never exceeded the initial set tube temperature. This temperature profile is denoted as 'initial cooling, slow exothermic reaction'. The temperature profile where HAN had an initial cooling effect on the tube, followed by heating past the initial set tube temp, is denoted as 'initial cooling, fast exothermic reaction'. Figures 24 and 25

show the 'initial cooling, slow exothermic reaction' and 'initial cooling, fast exothermic reaction' profiles, respectively.

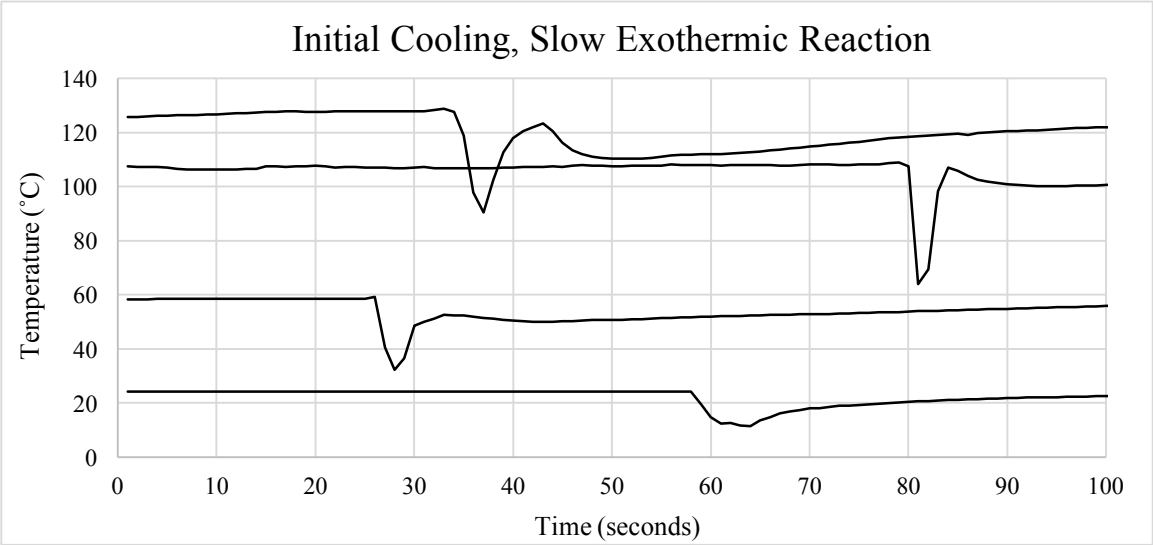

Figure 24: Temperature profiles of liquid feedthrough, 'initial cooling, slow exothermic reaction'

For each temperature profile, the maximum amount of NO produced was averaged and normalized by H_2O. The results are shown in Figure 26. The exponential trend seen in Figure 22 is also seen in Figure 26 for the three temperature profiles.

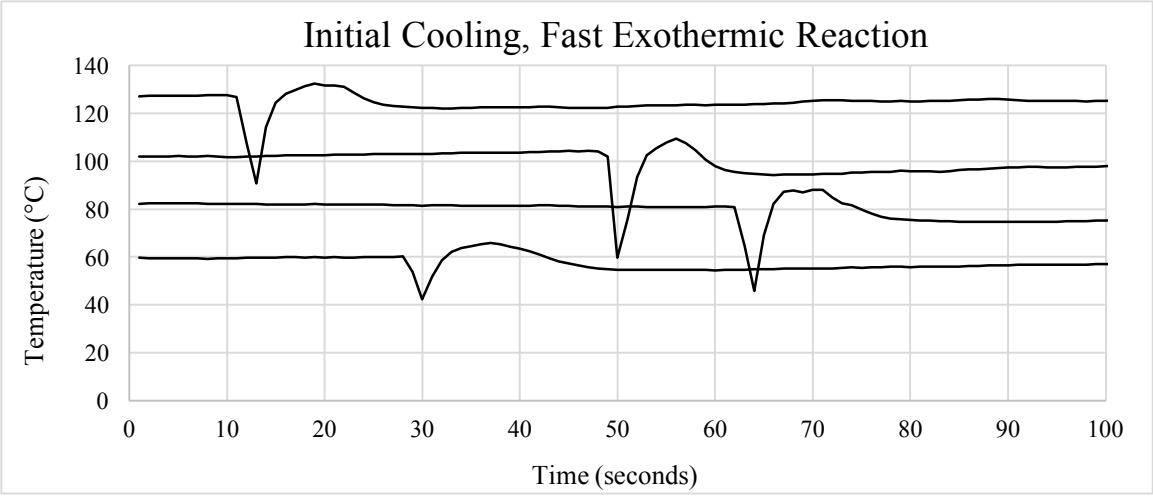

Figure 25: Temperature profiles of liquid feedthrough, 'initial cooling, fast exothermic reaction'

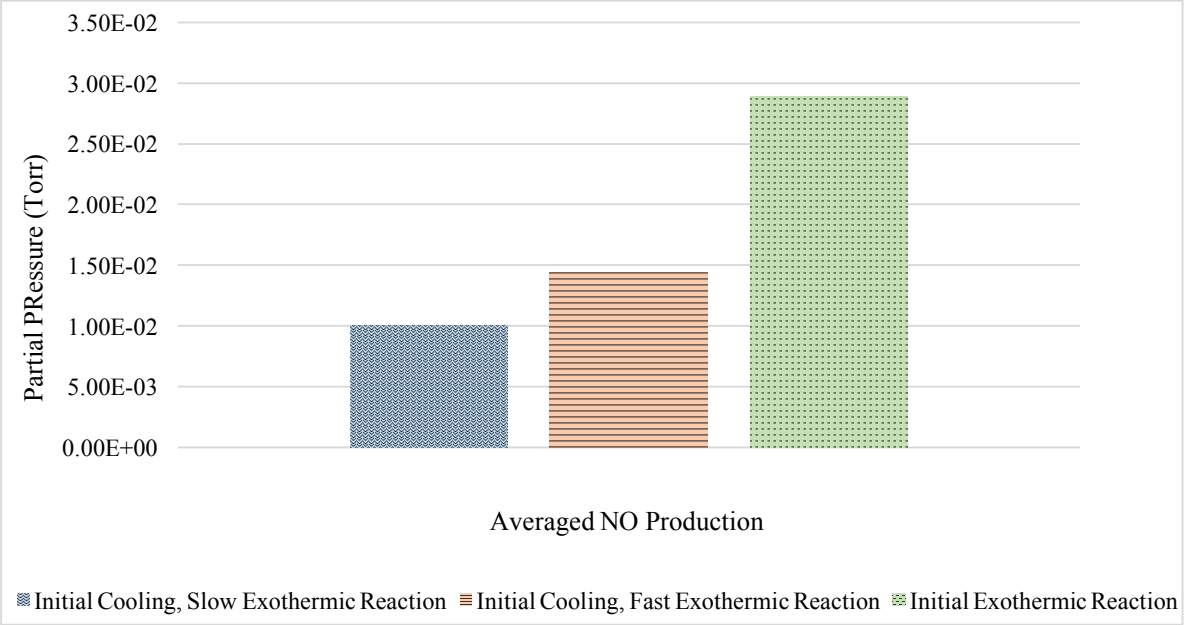

Figure 26: Averaged amount of NO produced for a given temperature profile

The 'initial exothermic reaction' profile resulted in an average partial pressure of 2.89E-2 Torr. This is two times the production from the 'initial cooling, fast exothermic reaction' profile, which resulted in an average partial pressure of 1.44E-2 Torr. The 'initial cooling, slow exothermic reaction' profile resulted in 1.00E-2 Torr for the averaged partial pressure of NO produced.

There is a slight correlation between the temperature profiles and the initial temperature, whereas at higher set temperatures, the 'initial exothermic reaction' profile dominated. This exothermic reaction is likely the self-catalytic and auto-decomposition that has been reported in previous studies, but the trigger for this reaction is still undetermined. However, previous studies have shown that HNO_3 can aid in the decomposition of HAN [21], [32], [33]. Furthermore, in this study, it was shown that HNO_3 develops as a result of vacuum conditions. Regardless of the decomposition mechanism, the gaseous products from the decomposition of HAN at increased temperature and initial low pressures, result in different amounts of the same gaseous species.

There is a significant amount of error associated with Figure 26. The following error values are calculated using standard deviation. The 'initial cooling, slow exothermic reaction' has a ±156% error; the 'initial cooling, fast exothermic reaction' has a ± 82% error; and the 'initial exothermic reaction' has a ±76% error. This error is a result of high variation in NO production within the temperature profiles.

Figure 27 provides a reference for the average set, average maximum, and average minimum temperatures of the tube. The exothermic reaction, which increased the maximum temperature, averaged higher for higher set temperatures, based on the categorization of temperature profiles. An increase in heat relates to an increased production of NO. And the produced NO is more related to the max temperature than the set temperature of the tube. However, the NO production cannot be directly correlated to the increase in temperature. It is possible that the reaction itself could produces NO, independent of temperature.

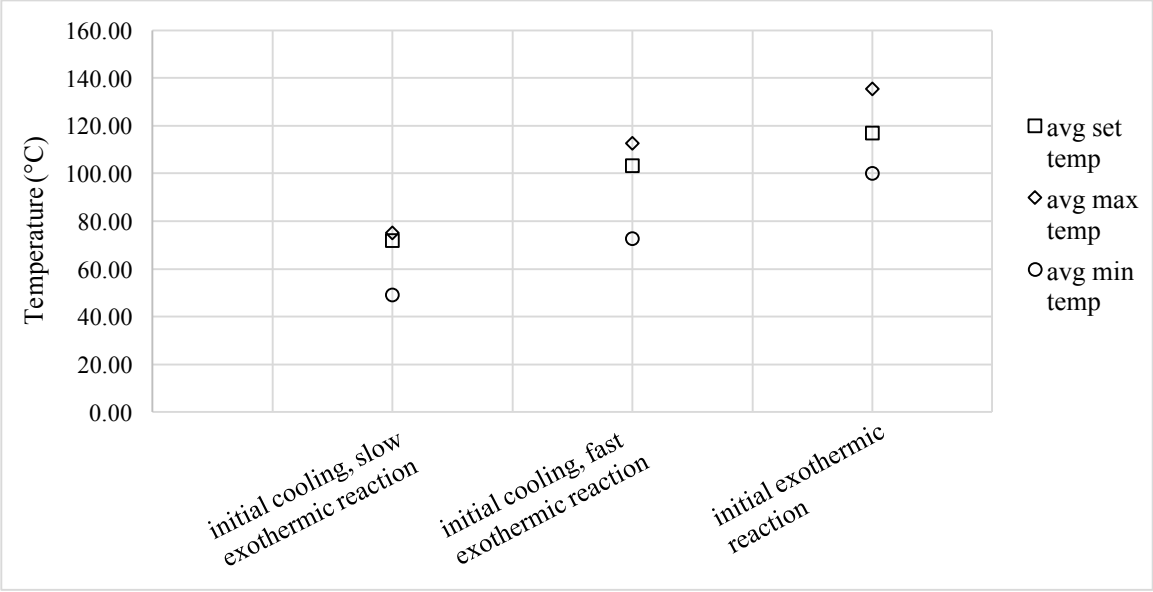

Figure 27: Average set, maximum, and minimum temperatures for each temperature profile

Each point given in Figure 27 is associated with an error percentage based on calculated standard deviations. Table 6 below shows the error percentage for each point. The error is

caused by the large amount of variation within each temperature profiles, as seen by Figures 23-25. The difference in error for each profile shows that there is more variation at lower temperatures than at higher temperatures.

Table 6: Error percentages for Figure 27

	Initial Cooling, Slow Exothermic Reaction	Initial Cooling, Fast Exothermic Reaction	Initial Exothermic Reaction
Avg Set Temp	± 60%	± 28%	± 18%
Avg Max Temp	± 63%	± 29%	± 21%
Avg Min Temp	± 93%	± 35%	± 32%

The majority of the experiments done in this research were performed at low pressure between 6.0E-3 and 6.43E-2. However, higher pressure values of 0.7 and 4 Torr were also investigated to see if higher pressures had any significant effect on the decomposition products. The maximum pressure used was 4 Torr, due to limitations on the RGA system. The RGA filament must remain at 1.0E-4 Torr or lower for safe operation. The pressure difference from the DC to the vacuum chamber was not an issue; however, the pressure in the vacuum chamber became too high for the RGA past 4 Torr despite the presence of the differential pumping system. The change in pressures from 6.0E-3 to 6.43E-2 was a result of remaining water in the DC. The pressures of 0.7 and 4 Torr were a result of backfilling the DC with Argon.

Figures 28 and 29, with partial pressure on the Y axis as a log scale, and initial DC pressure on the X axis as a log scale, show the maximum amount of NO and N_2O produced, respectively. All data are normalized by the maximum water produced during each experiment. Figures 28 and

29 organize the data by set tube temperature, not the max tube temperature resulting from the possible rise in temperature.

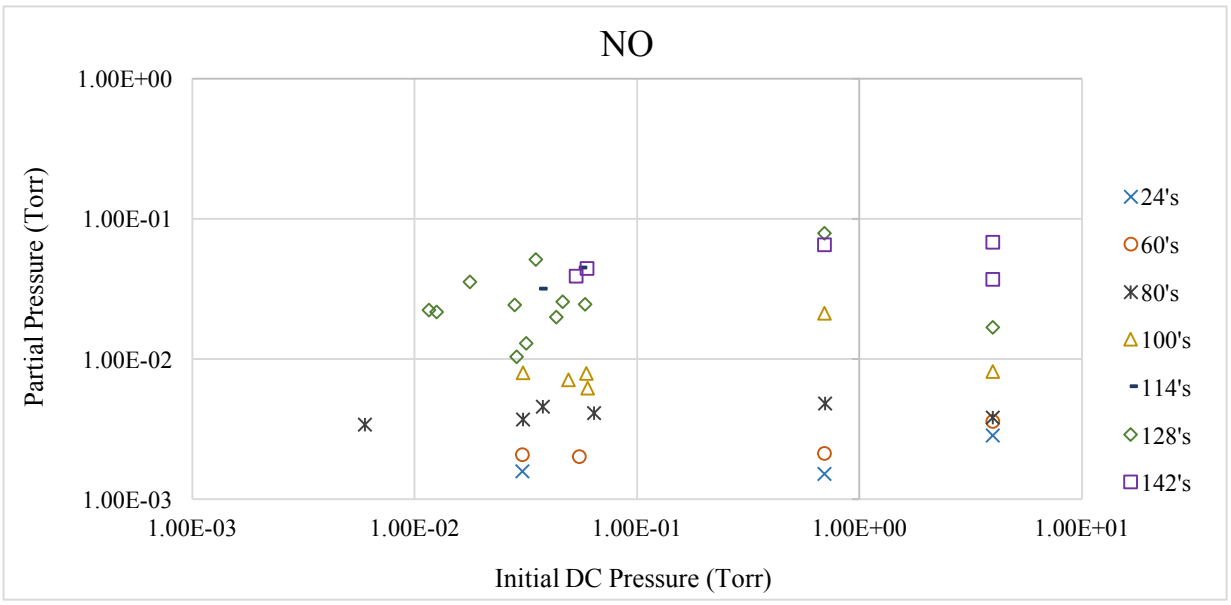

Figure 28: NO production at various set temperatures as a function of initial DC pressure

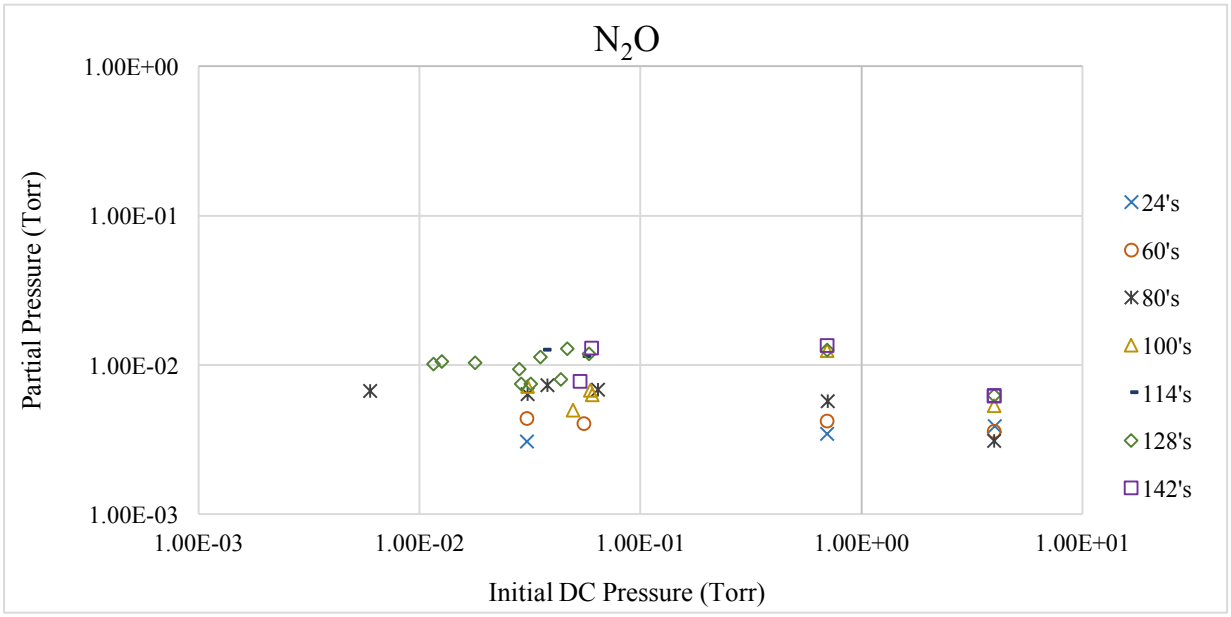

Figure 29: N_2O production at various set temperatures as a function of initial DC pressure

The production of NO and N_2O across the pressure range investigated suggests that pressure has no effect on the decomposition products. The figures also show that an increase in

temperature still increases NO production at higher pressures and that temperature has a lesser effect on N_2O production for the same pressure set points. The pressure in the DC did not stay at the initial pressure when the valve to the HAN was opened. The introduction of water and HAN caused the pressure to rise; and therefore, the effects of vacuum on HAN are limited to its initial exposure.

Solid HAN Heated under Vacuum

When using Experimental Setup 2, the environment affecting HAN changes more drastically. The effect of quickly reducing the pressure freezes the HAN-water solution through evaporative cooling. The upper right photograph in Figure 30 shows frozen HAN drops on the heater screen, whereas the upper left photograph shows the HAN-water solution prior to pumping. HAN slowly melts as the screen returns to room temperature after the initial evaporation of water from the solution. Eventually, and with the help of the turbo pump, enough water is removed to create solid HAN. Solid HAN and highly concentrated liquid HAN are present on the heater screen simultaneously as seen in the lower left picture of Figure 30. With the addition of heat, the solid,

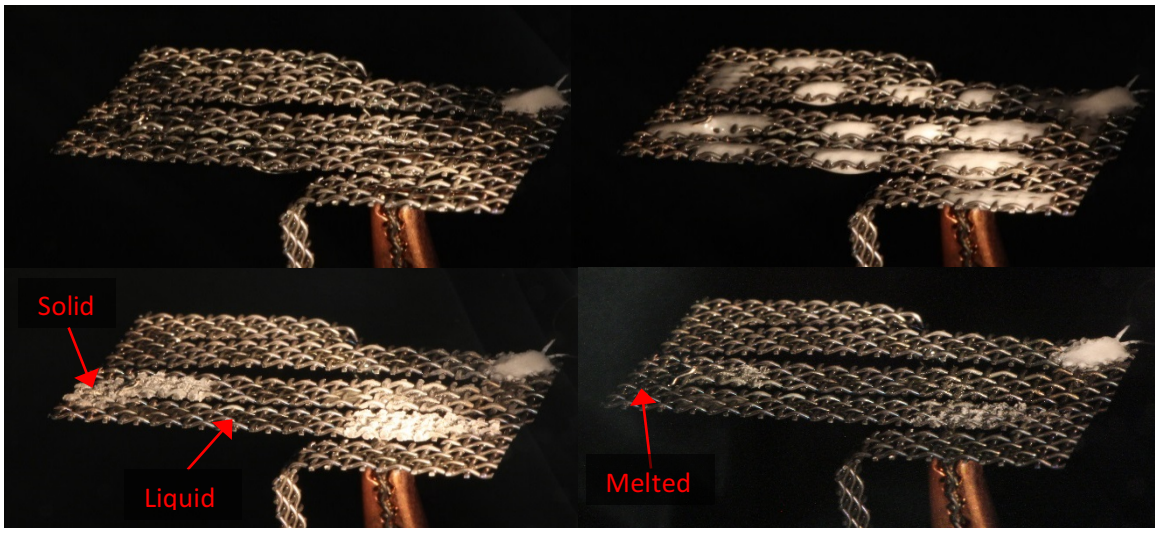

Figure 30: Photographs of HAN as pressure is reduced. Upper left: HAN-water solution, upper right: frozen HAN-water solution, lower left: solid and liquid HAN, lower right: partially melted HAN

crystalized HAN melts into highly concentrated liquid HAN as shown in the bottom right photograph in Figure 30. It is assumed that the majority of water has been removed from the initial HAN-water solution due to the background pressure before heat was applied to the HAN.

Three experiments were conducted using Experimental Setup 2, where HAN was deposited onto a heater screen under atmospheric conditions, low pressure was achieved inside the vacuum chamber, and then slowly heated. For these experiments, the RGA scan began once the vacuum chamber was at a low enough pressure to allow for RGA operation. Any decomposition from the effect of vacuum before the RGA scan began is unknown. However, previous results from this work shown HAN decomposition prior to the use of the turbo pump. Once solid HAN formed on the heater screen, the heater was turned on and the screen temperature was slowly increased.

Figure 31 indicates that the RGA spectra starts with the temperature of HAN at 23°C; the chamber pressure at 1.8E-5 Torr; water at a partial pressure of 2.6E-7 Torr; and NO present with a partial pressure of 9.0E-8 Torr. The temperature was slowly increased, as seen by the red line of Figure 31.

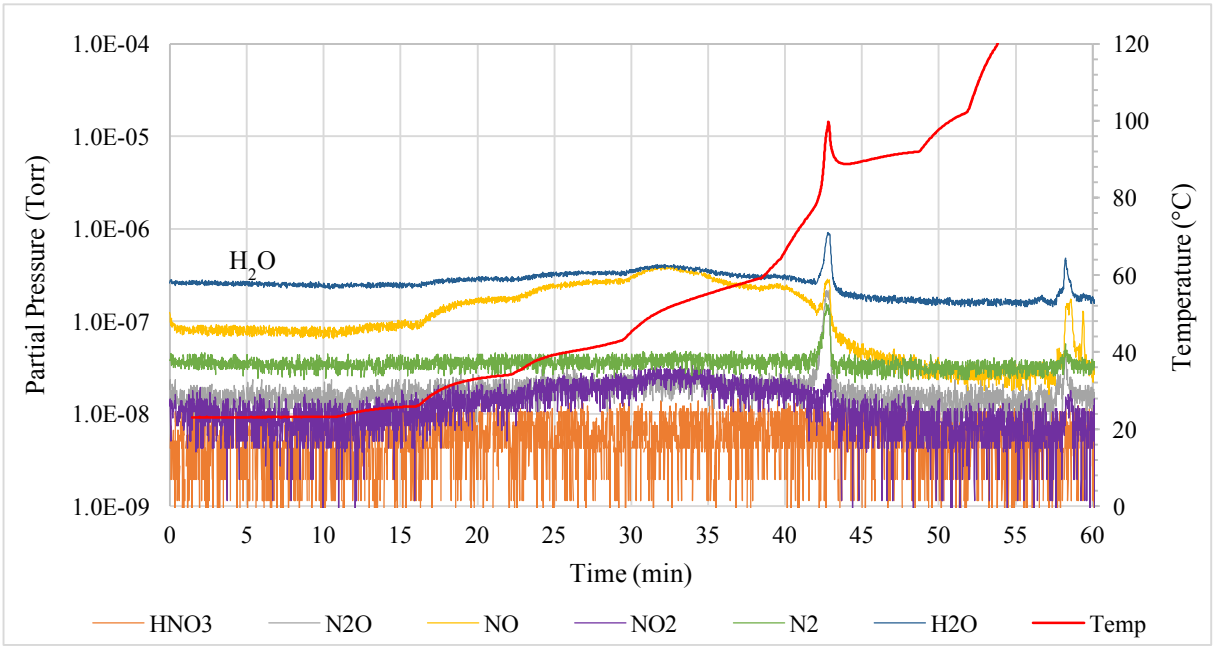

Figure 31: RGA partial pressure vs. time scan and temperature data

As a result of slowly applying heat, NO, H_2O, and trace amounts of N_2O and NO_2 form. An auto-decomposition reaction occurred as a result of the increased HAN temperature and therefore, the partial pressures of H_2O, NO, N_2O, N_2, and NO_2 increased. Without changing the heater power, auto-decomposition occurred at a temperature close to 80°C, resulting in an increase in temperature of about 20°C. At the end of the experiment, the temperature was increased to 625°C in attempts to clear any remaining HAN from the screen, as shown by the small spike in decomposition products around 58 minutes in Figure 31.

Figure 32 depicts a repeat of the previous experiment. HAN was deposited onto the heater screen while at atmosphere, and the chamber was evacuated to 1.8E-5 Torr before heating. The RGA scan began with H_2O and NO present with the partial pressures of 2.3E-7 Torr and 6.6E-8 Torr, respectively, and a heater screen at 23°C.

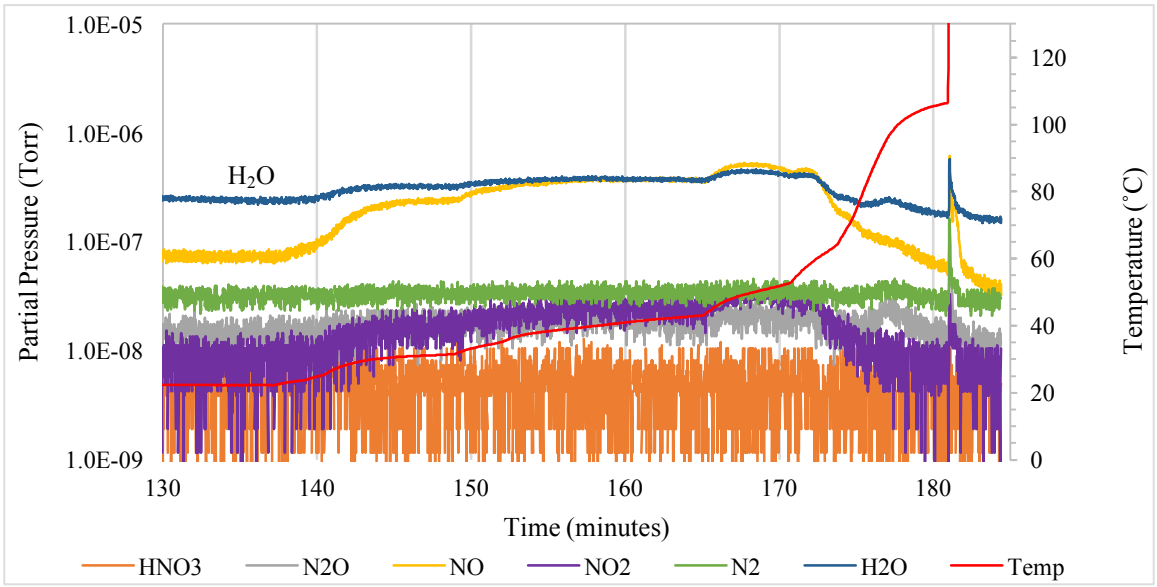

Figure 32: RGA partial pressure vs. time scan and temperature data

As the temperature of the heater screen increased, the presence of H_2O and NO increased. There is also a slight increase in NO_2 and N_2O as a result of heating. Auto-decomposition did not occur, or was not noticeable during this experiment. The large spike in partial pressure near a time

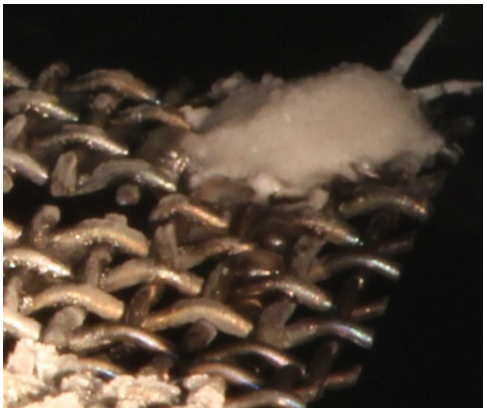

Figure 33: Picture of discolored, bubbling HAN under heated conditions

of 181 minutes in Figure 32 was a result of heating HAN to 640°C, and produced H_2O, NO, N_2O, N_2, and NO_2. Interestingly, the partial pressures of the decomposition products that resulted from the temperature increase are similar to the decomposition products resulting from auto-decomposition. During the slow heating of HAN, a reaction was visually observed on the heater screen. In Figure 33, the HAN appears to have a brownish hue and to be forming bubbles. The reaction occurred as a result of slight heating; however, there was insufficient heat to melt all of the crystalized HAN. This reaction was likely caused by contaminates on the heater screen from past experiments.

The experiment shown in Figure 34 was conducted using a new heater screen. The RGA scan began with a chamber pressure of 2.75E-5 Torr, water at a partial pressure of 2.61E-7 Torr, and NO with a partial pressure of 3.94E-8 Torr. The thermocouple was not reading correctly due to a loose wire so the precise temperature of the screen prior to heating is unknown; however, it is assumed to be at room temperature, ~23°C, based on previous experiments. Again, the temperature was slowly increased, as seen by the red line. As a result of heating, H_2O and NO were prominent, with NO_2 and N_2O observed in trace amounts. Auto-decomposition occurred with the heater screen

at 78°C at a time of 124.5 minutes and resulted in an increased partial pressure of H_2O, NO, N_2O, N_2, and NO_2. Also, no discoloration or bubbling was observed on the new, unused heater screen.

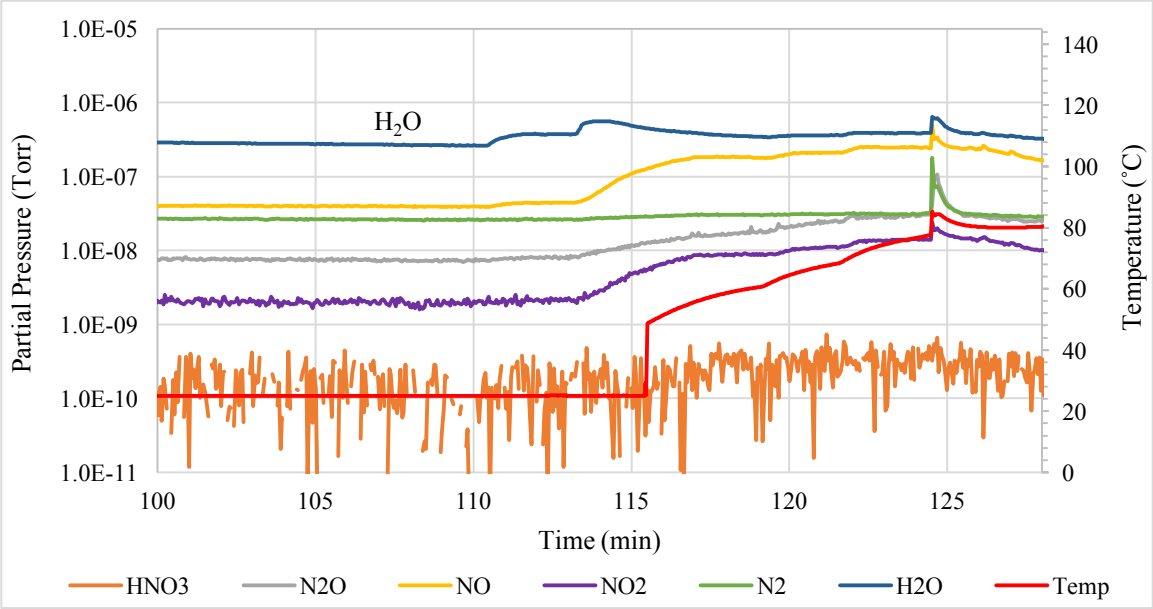

Figure 34: RGA partial pressure vs. time scan and temperature data

In all three experiments, NO is present in the vacuum chamber prior to heating. This seems to be a result of the low pressure and possible increase in HAN concentration. When heat is applied, these experiments demonstrate an increase in NO and H_2O, where H_2O is either a decomposition product or a result of the remaining water in the HAN being evaporated. Due to the low pressures achieved and the observed partial solid state of HAN prior to heating, it is more likely a decomposition product. For Figures 31 and 34, a temperature close to 80˚C begins the runaway reaction described in the Literature Review. The concentration of HAN at the point of auto decomposition is unknown; however, the partial pressure of H_2O in both cases is equal, and therefore similar concentrations of HAN were present before heating. Summarized below in Table 7 are the decomposition products from all three experiments. The resultant gases are given in percent composition relative to the total partial pressure at the time of decomposition.

Table 7: Summary of auto-decomposition products

	% Decomposition Products					
	N_2O	NO	NO_2	N_2	H_2O	TOTAL
Figure 31	11.8	17.0	1.42	8.68	54.8	93.7
Figure 32	9.57	37.9	2.05	10.2	35.6	95.2
Figure 34	2.75	32.7	1.58	11.9	42.7	91.6

The values in Table 7 are calculated from the maximum partial pressure of each gas during auto-decomposition. The decomposition products do not equal 100% because other gases are present inside the chamber, such as hydrogen and oxygen, which are not related to decomposition, and are therefore not shown in the table. Looking at Table 7, H_2O is the primary decomposition product followed by NO. The gaseous species NO_2 and N_2 are fairly consistent for all three experiments, whereas N_2O has greater variation. Due to fragmentation, almost 60% of NO_2 produced from decomposition registers as NO on the RGA, and only 22% of NO_2 is seen as such. As a result, the compositions shown in the table are approximations. The reason for the differences in decomposition product percentages is unclear. However, the heater screen used in Figure 34 was a previously unused, uncontaminated heater screen, whereas the heater screen used in in the two prior experiments had been used previously with HAN. The decomposition process may have been affected by the presence of residual contaminates on the screen. The solid byproduct of HAN decomposition, if any, is unknown. However, HNO_3 is likely formed within HAN as it decomposed, and residual HNO_3 on the heater screen may have affected proceeding experiments.

CHAPTER VI

CONCLUSION

Discussion

The gaseous decomposition products of HAN under vacuum conditions are N_2O, NO, NO_2, H_2O, and N_2. The formation of N_2O occurs primarily when HAN is initially exposed to vacuum. It is hypothesized that HAN under vacuum follows Reaction 5 as shown previously.

$$4\,NH_3OH^+\,NO_3^- \rightarrow\ 3\,N_2O +\ 2\,HNO_3 +\ 7\,H_2O \qquad \text{(R5)}$$

The longer HAN is exposed to vacuum, the less prevalent N_2O formation becomes. As a result of HAN being heated, NO is produced. Heating HAN when in solution with water, or as a highly concentrated solid-liquid, results in primarily NO; and therefore it is hypothesized that heated HAN follows Reaction 6.

$$NH_3OH^+\,NO_3^- \rightarrow 2\,NO + 2\,H_2O \qquad \text{(R6)}$$

NO_2 is produced in trace amounts from exposing HAN to vacuum, heating HAN under vacuum, and as a result of auto-decomposition. HAN decomposition under lower levels of vacuum demonstrated no change on the decomposition products. The increased pressure also had no significant effect on the relative amounts of resultant gaseous species produced. Notably, the vacuum pressures in which HAN was exposed to in Experimental Setups 1 and 1B, acted only on the HAN-water solution momentarily, until the presence of the liquid itself raised the pressure.

From previous experimental studies, as well as proposed HAN decomposition reactions, H_2O and N_2 are plausible decomposition products. The experiments which involved exposing HAN to vacuum, and heating HAN under vacuum in the DC, provided inconclusive results on the

formation of H_2O and N_2. Water from the HAN solution, and the air in the ball valve, may have been the only source of H_2O and N_2, and not the decomposition of HAN. However, when HAN was used in Experimental Setup 2, the presence of solid-liquid HAN suggests that the majority, if not the totality of water was removed from the HAN-water solution. Further heating of the solid-liquid HAN resulted in primarily NO and H_2O. Furthermore, the auto-decomposition that occurred as a result of an increase in temperature, resulted in a strong spike in H_2O as well as a spike in N_2. The formation of H_2O and N_2 under these circumstances suggests that they are decomposition products, even though the formation was not clearly observed when using Experimental Setups 1 and 1B. The decomposition of HAN under vacuum conditions is conditional on the process by which HAN decomposes. Inducing an auto-catalytic reaction will produce different resultant gaseous species than slowly applying heat. Applying heat rapidly to highly concentrated HAN, as seen in Figure 32, produces the same products as those produced from auto-decomposition.

In addition to the formation of these decomposition gases, the formation of HNO_3 was detected in trace amounts using the RGA. The formation of HNO_3 was observed as a result of both exposing HAN to vacuum and heating HAN under vacuum, but not as a result of auto-decomposition. According to previous experimental studies, HNO_3 forms easily in HAN as a result of a proton transfer forming hydroxylamine and HNO_3, nitric acid [19]. Previous studies also suggest that HNO_3 accelerates the decomposition of HAN [13]. Consequently, the presence of HNO_3 on or within the experimental setups may have had an effect on the decomposition of HAN. This possibility was realized late in the experimental procedure, and therefore little corrective course was taken. The possible formation of HNO_3 was detected when HAN underwent a color change to a brownish hue, coupled with bubbling. This reaction took place under vacuum conditions in an attempt to induce auto-decomposition by adding heat. After replacing the heater

screen, and repeating the experiment, no such reaction occurred. The reaction was a possible result of HNO_3, or some other contaminant on the heater screen from past HAN experiments. However, no data other than observational data can support this hypothesis. A further investigation should be conducted.

The error percentages calculated for Figure 26 show that there is significant variation in NO production for all three temperature profiles. The error associated with Figure 27 shows that there is significant variation with the temperature profiles. Furthermore, the decrease in error from 'initial cooling, slow exothermic reaction' to 'initial cooling, fast exothermic reaction' and continuing to 'initial exothermic reaction' suggests that there is less variation for profiles of higher temperatures.

The RGA ionizer setting of 70 eV was constant for all experiments reported in this paper. The effects of fragmentation due to the ionizer setting are present in all partial pressure data. Subsequently, all resultant gaseous species produced as a result of varying conditions can be compared without considering fragmentation. However, when comparing the amount of gas produced within a given experiment, fragmentation must be taken into account. N_2O fragments primarily into NO, and as a result, the reported partial pressure of NO will be less than the measured partial pressure by the RGA. Similarly, NO_2 and N_2O exists in greater quantities than what was reported.

Future Work

This work is meant to be a stepping-stone in completely understanding the decomposition of HAN-based ionic liquid propellants. A specific HAN-based ionic liquid propellant is also composed of the ionic liquid HEHN; and therefore, this research should be repeated using HEHN and mixtures of HAN and HEHN. These additional experiments should be conducted using the

experimental setup used in this thesis, which employs an RGA, and should also employ an FT-IR diagnostic system. Additionally, the FT-IR should be used to investigate the decomposition of HAN to help verify the results measured by the RGA.

After the investigation into other HAN-based ionic liquids, the ionization of the resultant gaseous species of those HAN-based ionic liquids needs to be studied. The ionization of complex molecular components needs to be understood in order to successfully develop a gas-phase electric propulsion device using ionic liquids as the propellant.

Future experiments should also include an experiment using nitric acid and HAN to study the effects of nitric acid on HAN under vacuum conditions. Nitric acid is believed to be a by-product of HAN decomposition under certain conditions. However, the experiments conducted in this thesis were unable to conclude if nitric acid was formed and led to possible contamination issues.

Recommendations

After considering the work done in this thesis alongside the application of a gas-phase electric propulsion device, it is recommended that the ionic liquid be decomposed in a high temperature, standard pressure or higher environment. Based on the results, decomposition of HAN begins when it is subjected to vacuum. Additionally, varying levels of heat generate varying levels of decomposition gasses. Therefore, a high-pressure environment along with a high temperature environment should prevent partial decomposition from occurring. This decomposition already occurs in the decomposition chamber of monopropellant thrusters; and it is therefore recommended that the propellant for a gas-phase electric propulsion device be the resultant gaseous species from thermal and catalytic decomposition.

BIBLIOGRAPHY

[1] F. Kamal, B. Yann, B. Rachid, and K. Charles, *Application of Ionic Liquids to Space Propulsion*. InTech, 2011.

[2] A. S. Gohardani, J. Stanojev, A. Demairé, K. Anflo, M. Persson, N. Wingborg, and C. Nilsson, "Green space propulsion: Opportunities and prospects," *Prog. Aerosp. Sci.*, vol. 71, pp. 128–149, 2014.

[3] R. E. N. Xiaoguang, L. I. Minghui, W. Aiqin, L. I. Lin, W. Xiaodong, and Z. Tao, "Catalytic Decomposition of Hydroxyl Ammonium Nitrate at Room Temperature," *Chinese J. Catal.*, vol. 28, no. 1, pp. 1–2, 2007.

[4] L. Courtheoux, D. Amariei, S. Rossignol, and C. Kappenstein, "Thermal and catalytic decomposition of HNF and HAN liquid ionic as propellants," *Appl. Catal., B*, vol. 62, no. 3–4, pp. 217–225, 2006.

[5] S. A. Whitmore, D. P. Merkley, S. D. Eilers, and M. I. Judson, "Development and Testing of a Green Monopropellant Ignition System," *49th AIAA/ASME/SAE/ASEE Jt. Propuls. Conf.*, no. July, pp. 1–28, 2013.

[6] C. H. Hwang, S. W. Baek, and S. J. Cho, "Experimental investigation of decomposition and evaporation characteristics of HAN-based monopropellants," *Combust. Flame*, vol. 161, no. 4, pp. 1109–1116, 2014.

[7] R. Amrousse, K. Hori, W. Fetimi, and K. Farhat, "HAN and ADN as liquid ionic monopropellants: Thermal and catalytic decomposition processes," *Appl. Catal. B Environ.*, vol. 127, no. 2, pp. 121–128, 2012.

[8] H. S. Lee and T. A. Litzinger, "Thermal decomposition of han-based liquid propellants," *Combust. Flame*, vol. 127, no. 4, pp. 2205–2222, 2001.

[9] M. M.-T. Tsay, D. Lafko, J. Zwahlen, and W. Costa, "Development of Busek 0.5N Green Monopropellant Thruster," *Small Satell. Conf.*, pp. 1–6, 2013.

[10] R. A. Spores, "GPIM AF-M315E Propulsion System," *51st AIAA/SAE/ASEE Jt. Propuls. Conf.*, pp. 1–12, 2015.

[11] R. S. Jankovsky, "HAN-Based Assessment Monopropellant for Spacecraft," *NASA Rep.*, 1996.

[12] C. Oommen, S. Rajaraman, R. A. Chandru, and R. Rajeev, "Catalytic Decomposition of Hydroxylammonium Nitrate Monopropellant," *Proc. Int. Conf. Chem. Chem. Process (ICCCP 2011)*, vol. 10, pp. 205–209, 2011.

[13] V. D. Rafeev and Y. L. Rubtsov, "Kinetics and mechanism of thermal decomposition of hydroxylammonium nitrate," *Russ. Chem. Bull.*, vol. 42, no. 11, pp. 1811–1815, 1993.

[14] C. A. Van Dijk and R. G. Priest, "Thermal Decomposition of Hydroxylammonium Nitrate at Kilobar Pressures," *Combust. Flame*, vol. 57, no. 1, pp. 15–24, 1984.

[15] B. R. Donius and J. L. Rovey, "Ionic Liquid Dual-Mode Spacecraft Propulsion Assessment," *J. Spacecr. Rockets*, vol. 48, no. 1, pp. 110–123, 2011.

[16] N. Klein, "Liquid Propellants for Use in Gun - A Review," Aberdeen Proving Ground, Maryland, 1985.

[17] C. Wei, W. J. Rogers, and M. S. Mannan, "Thermal decomposition hazard evaluation of hydroxylamine nitrate.," *J. Hazard. Mater.*, vol. 130, no. 1–2, pp. 163–8, 2006.

[18] L. Liu, C. Wei, Y. Guo, W. J. Rogers, and M. Sam Mannan, "Hydroxylamine nitrate self-catalytic kinetics study with adiabatic calorimetry," *J. Hazard. Mater.*, vol. 162, no. 2–3, pp. 1217–1222, 2009.

[19] J. Oxley and K. Brower, "Oxley, Brower - 1988 - Thermal Decomposition of Hydroxylamine Nitrate.pdf," *Proc. SPIE Int. Soc. Opt. Eng.*, vol. 872, pp. 63–69, 1988.

[20] R. W. Ashcraft, S. Raman, and W. H. Green, "Predicted reaction rates of H(x)N(y)O(z) intermediates in the oxidation of hydroxylamine by aqueous nitric acid.," *J. Phys. Chem. A*, vol. 112, no. 33, pp. 7577–93, 2008.

[21] R. W. Ashcraft, S. Raman, and W. H. Green, "Ab initio aqueous thermochemistry: application to the oxidation of hydroxylamine in nitric acid solution.," *J. Phys. Chem. B*, vol. 111, no. 41, pp. 11968–83, 2007.

[22] C. Zhang, “Thermal Decomposition Study of Hydroxylamine Nitrate During Storage and Handling Thermal Decomposition Study of Hydroxylamine Nitrate During Storage and Handling,” no. May, 2006.

[23] C. Wei, “Thermal Runaway Reaction Hazard and Decomposition Mechanism of the Hydroxylamine System Thermal Runaway Reaction Hazard and Decomposition Mechanism of the Hydroxylamine System,” Texas A&M University, 2005.

[24] R. Amrousse, T. Katsumi, N. Itouyama, N. Azuma, H. Kagawa, K. Hatai, H. Ikeda, and K. Hori, “New HAN-based mixtures for reaction control system and low toxic spacecraft propulsion subsystem: Thermal decomposition and possible thruster applications,” *Combust. Flame*, vol. 162, no. 6, pp. 2686–2692, 2015.

[25] R. Amrousse, T. Katsumi, T. Sulaiman, B. R. Das, H. Kumagai, K. Maeda, and K. Hori, “Hydroxylammonium Nitrate As Green Propellant: Decomposition and Stability,” *Int. J. Energ. Mater. Chem. Propuls.*, vol. 11, no. 3, pp. 241–257, 2012.

[26] H. Lee and T. A. Litzinger, “Chemical kinetic study of HAN decomposition,” *Combust. Flame*, vol. 135, no. 1, pp. 151–169, 2003.

[27] J. W. Schoppelrei and T. B. Brill, “Spectroscopy of Hydrothermal Reactions. 7. Kinetics of Aqueous [NH 3 OH]NO 3 at 463-523 K and 27.5 MPa by Infrared Spectroscopy,” vol. 101, no. 3, pp. 8593–8596, 1997.

[28] R. Amrousse, T. Katsumi, N. Itouyama, N. Azuma, H. Kagawa, K. Hatai, H. Ikeda, and K. Hori, “New HAN-based mixtures for reaction control system and low toxic spacecraft propulsion subsystem: Thermal decomposition and possible thruster applications,” *Combustion and Flame*, vol. 162, no. 6. pp. 2686–2692, 2015.

[29] J. M. Hollas, *Modern Spectroscopy*, 4th ed. John Wiley & Sons, Ltd, 2004.

[30] SRS, “Operating Manual and Programming Reference: Modles RGA100. RGA200, RGA300 Residual Gas Analyzer,” vol. 8. 2009.

[31] P. J. Lindstrom and W. G. Mallard, Eds., “NIST Chemistry WebBook, NIST Standard Reference Database Number 69,” National Institute of Standards and Technology, Gaitherburg, MD, 20899, http://webbook.nist.gov, (retrieved February 25, 2016).

[32] J. R. Pembridge and G. Stedman, “Kinetics, Mechanism, and Stoicheiometry of the Oxidation of Hydroxylamine by Nitric Acid,” *J. Chem. Soc. Dalt. Trans.*, pp. 1657–1663, 1979.

[33] R. J. Gowland and G. Stedman, “Kinetic and Product Studies on the Decomposition of Hydroxylamine in Nitric Acid,” vol. 43, no. 11, pp. 2859–2862, 1981.